ADVANCED HEALTHCARE MATERIALS
www.advhealthmat.de

Bone Tissue Engineering Scaffolds: Function of Multi-Material Hierarchically Structured Scaffolds

*Tejas M. Koushik, Catherine M. Miller, and Elsa Antunes**

Bone tissue engineering (BTE) is a topic of interest for the last decade, and advances in materials, processing techniques, and the understanding of bone healing pathways have opened new avenues of research. The dual responsibility of BTE scaffolds in providing load-bearing capability and interaction with the local extracellular matrix to promote bone healing is a challenge in synthetic scaffolds. This article describes the usage and processing of multi-materials and hierarchical structures to mimic the structure of natural bone tissues to function as bioactive and load-bearing synthetic scaffolds. The first part of this literature review describes the physiology of bone healing responses and the interactions at different stages of bone repair. The following section reviews the available literature on biomaterials used for BTE scaffolds followed by some multi-material approaches. The next section discusses the impact of the scaffold's structural features on bone healing and the necessity of a hierarchical distribution in the scaffold structure. Finally, the last section of this review highlights the emerging trends in BTE scaffold developments that can inspire new tissue engineering strategies and truly develop the next generation of synthetic scaffolds.

1. Introduction

Bone is a multifaceted tissue that provides structural support while simultaneously contributing to critical biological functions that keep us alive and functioning. It protects our soft tissues from the physical trauma endured while doing daily tasks. However, like any other human body tissue, defects or accidents can severely damage bone tissues beyond self-recovery. While the bone tissue has a self-healing ability, it is only capable of regenerating and remodeling small (<6 mm) defects/damages but remains insufficient for larger defects.[1]

The gold standard for the recovery of larger fractures involves using autologous grafts derived from human donors. The limited supply of autologous grafts has seen the development of studies focusing on developing novel bone tissue engineering (BTE) strategies for bone regeneration.[2] Scaffolds used for BTE applications must be designed, taking into consideration their structural capacity and interaction with the extracellular matrix (ECM). For example, the foreign body response is triggered due to the preferential adsorption of fibrin onto the implant's surface.[3] Neutrophils in the implant area attract monocytes to the fibrin-dominated implant surface, which subsequently differentiate into macrophages, releasing pro-inflammatory factors such as tumor necrosis factor-alpha (TNF-α), interleukin-6 (IL-6), and interleukin-8 (IL-8). These macrophage populations at the injury site encapsulate the surface with fibrous tissue, preventing any further interaction with local ECM.[3] The inability to interact with the ECM prevents the transfer of ions and nutrients required for the damaged tissue to undergo osseointegration. Lack of osseointegration could eventually require additional surgeries for removal, and therefore, compromise recovery in the long term. The specificity in fibrin adsorption could be due to the scaffold's surface charge, wettability, and chemical composition.[4] Thus, materials that positively interact with the local cells and initiate a bone-healing response must be chosen. Just like bone tissue, organic components present within their structure must interact with the cells around them while inorganic components enhance their structural strength. Similarly, BTE scaffolds must have a dual function of inducing positive healing processes while simultaneously supporting the damaged areas.

Osteoinductivity, osteoconductivity, and biocompatibility of the scaffold are the three critical requirements of BTE scaffolds. Osteoinduction refers to the ability of scaffolds to recruit the host mesenchymal stem cells (MSCs) from surrounding tissues and differentiate them into osteoblast cells, which are responsible for bone growth.[5] Osteoconduction is the ability of the material to facilitate the growth of cells on the scaffold.[5] Biocompatibility,

T. M. Koushik, E. Antunes
College of Science and Engineering
James Cook University
Townsville, Queensland 4811, Australia
E-mail: elsa.antunes1@jcu.edu.au
C. M. Miller
College of Medicine and Dentistry
James Cook University
Smithfield, Queensland 4878, Australia

The ORCID identification number(s) for the author(s) of this article can be found under https://doi.org/10.1002/adhm.202202766

DOI: 10.1002/adhm.202202766

as described in the previous section, refers to the scaffold's ability to not trigger the foreign body response when implanted. In addition to these material properties, the scaffold's architecture (macrostructure and microstructure) will dictate the extent of angiogenesis achievable. The extent of angiogenesis is known to directly impact the extent of cell spreading, transportation of nutrients (blood, biomolecules, or waste), and bone in-growth.[6] Further, the hierarchical nature of the bone structure has a wide range of porosities depending on the type, location, and function.[7] Therefore, the scaffolds will require a range of porosities (size, shape, and extent) to function as effective BTE scaffolds.

Previous reviews have described the effects of material chemistry or processing techniques on the bone healing response;[8] however, these reviews have discussed the effects of a single material, whereas as discussed in this review, most scaffolds are comprised of multiple materials. Although using additives, such as signaling molecules, growth factors, stem cells, and other functional materials, has been a popular approach to supplement the regenerative pathways during bone healing, most recent review articles do not describe the regenerative pathways influenced by composite materials to improve bone healing ability.[9] Limitations of conventional techniques to manufacture next-generation tissue engineering scaffolds (biofunctionality, patient-specific, and degradable) have been previously discussed,[10] as well as the role and capabilities of additive manufacturing (AM) in the future of regenerative medicine.[11] However, previous review articles discussing AM for BTE applications are focused on the operational challenges and the strategies to overcome them.[12] Therefore, this review aims to highlight the synergistic effects of multi-materials and scaffold architecture on the bone healing response. The function of materials in the bone healing pathways, as well as structural features affecting bone healing, and the need to introduce hierarchy to enhance the adaptability and efficacy of these scaffolds are discussed. Conventional methods to manufacture porous material have been previously discussed extensively; thus, this review will only focus on techniques capable of producing hierarchical porosities and the ability to process multiple materials.

2. Scaffold Function in Bone Tissue Engineering

2.1. Structure of Bone Tissue

Bone is a living material that supports the musculoskeletal system, functions as a source of calcium, and stores the bone marrow. It is organized in a complex hierarchical structure extending from a few nanometers to micrometers, as shown in **Figure 1**I. The various cell types present in the ECM of these bone tissues enable them to repair and remodel themselves constantly. Osteoblasts, osteoclasts, bone lining cells, and osteocytes present at the injured site have specific functions responsible for initiating or sustaining the bone healing response. Osteoblasts are responsible for forming bone tissue by producing bone ECM components such as type I collagen, proteoglycans, non-collagenous proteins, and cell attachment proteins.[13] Matrix vesicles secreted by the osteoblasts and present in the ECM provide a nurturing environment for the nucleation of calcium phosphates. Mineralization of these vesicles begins when crystalline calcium phosphates appear inside them, this step is governed by transporter membranes and enzymes.[14] Osteoclasts are multi-nucleated cells derived from monocytes that are responsible for bone resorption in response to local stimuli.[15] The resorption process is critical in maintaining blood calcium levels.[16] Osteocytes are osteoblast cells surrounded by mineralized bone tissue.[16] The location and interconnectivity of these cells make them ideal for detecting and transducing mechanical stresses into a physiological response.[16] Osteogenic cells (bone lining cells) form a thin layer on bone tissues, functioning as a protective layer from further osteoclast activity. However, with suitable stimulation, they could form osteoblasts.[16] These osteogenic cell types are usually up to a few microns in size depending on their location and are the basic building blocks essential for the formation and maintenance of bone tissue.

Cell types (osteoblasts, osteoclasts, bone lining cells, and osteocytes) are responsible for the maintenance and repair of bone tissue. The supply of oxygen and nutrients for these cell types is critical to ensuring their survival. The diffusion limit for oxygen in tissues has been reported to be within the range of 100–200 μm, that is, oxygen diffusion will only occur in the tissues within 200 μm of the oxygen source.[17] The blood distributes oxygen and nutrients to bone tissues through capillaries. The hypoxic state of the cells at the injured site (due to the inflammatory wound healing response triggered after the injury) triggers the release of vascular endothelial growth factor (VEGF).[18] VEGF causes the differentiation of angioblasts into primitive blood vessels; this process is termed vasculogenesis and needs to occur prior to angiogenesis. Endothelial cells present within the tissue bridge the gaps between these primitive blood vessels to form capillary buds and sprouts; this process is defined as angiogenesis.[18]

The structural morphology of bone tissues can be divided into osteons, lamella, collagen fibers, and collagen fibrils, considering their relative sizes.[19] The collagen fibrils consist of several sub-nanometer type I collagen molecules that are discretely separated by plate-like hydroxyapatite (HAp) crystals and other impurities such as HPO_4, Na, Mg, and K.[20] The fibrils self-assemble into bundles and orient themselves in specific directions forming collagen fibers with a diameter between 3 and 7 μm.[21] The arrangement of these fibers concentrically forms osteons in the range of 10–500 μm.[21,22] When these fibers are concentrically arranged around Haversian canals, they form Haversian systems, which are 150–300 μm thick, as shown in Figure 1II. Differences in the arrangement of these components within the bone produce two types called cortical and trabecular bone, as shown in Figure 1-IIIa. Cortical bone consisting of concentrically distributed osteons forms the dense exterior of bones, as shown in Figure 1-IIId. Trabecular bone shown in Figure 1IIIb consists of a more open network, where the empty spaces are occupied by blood vessels and bone marrow. This hierarchical organization of bone tissue extends from a few nanometers to micrometers, as shown in Figure 1II.[21]

Synthetic scaffolds used for BTE provide the template for tissue formation and stimulate bone tissue regeneration through interaction with ECM. Most importantly, scaffolds are meant to mimic the local niche of the tissue being regenerated. Mimicking the local niche requires a scaffold to facilitate angiogenesis for transporting critical nutrients, waste, and biomolecules to the synthetic scaffold.[6] Osteogenesis, coinciding with the above process, is augmented with the successful vascularization of the

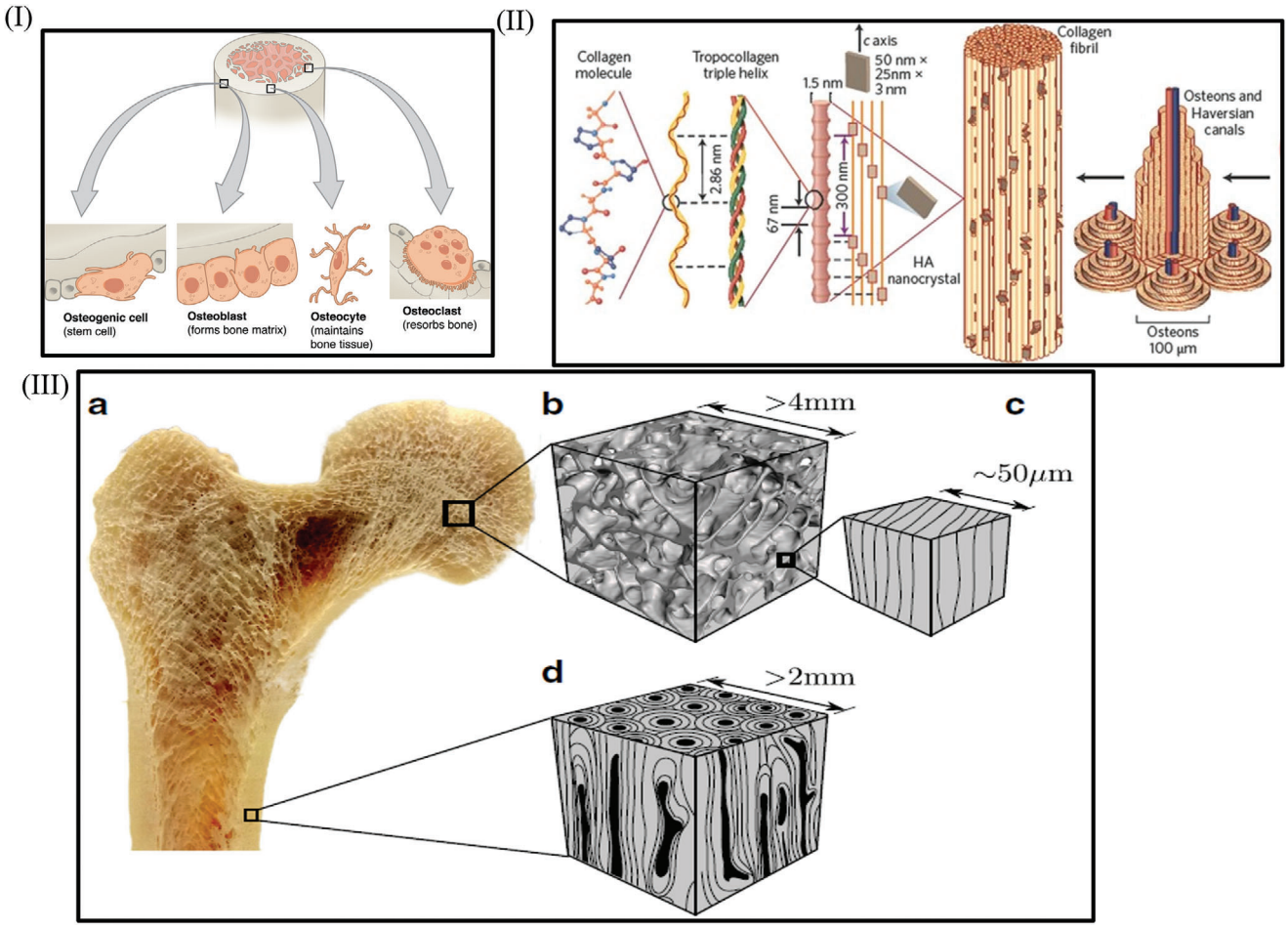

Figure 1. I) Each bone tissue consists of four cell types: osteoblasts, osteoclasts, osteocytes, and osteogenic cells (bone lining cells). Reproduced with permission.[23] Copyright 2022, Libretexts. II) Type I collagen is an abundant protein consisting of polypeptide chains that fold into triple-helical tropocollagen molecules. Tropocollagen molecules self-assemble into microfibrils, which aggregate in longitudinal and horizontal directions to form collagen fibrils. The collagen fibrils' dimensions vary within the bone structure.[19] Osteoblasts precipitate calcium and phosphate through the action of alkaline phosphatase on the phosphate and calcium groups available. Stoichiometry of the precipitated calcium and phosphate is highly dynamic and often changes depending on the required osteoclast activity.[7] The multi-scale features at different organizational levels show bone as a complex arrangement of multi-scale tissues. Reproduced with permission.[19] Copyright 2015, Springer Nature. III) The morphological distinction between trabecular and cortical bone a) representing the cross-section of the long bone, b) internal morphology of trabecular bone structures, c) arrangement of lamellae within the trabecular bone matrix, and d) arrangement of osteons in the cortical bone matrix. Reproduced with permission.[24] Copyright 2020, Springer Nature

synthetic scaffold. Physical attributes, such as pore size, porosity, pore structure, and interconnectivity of the scaffold, are crucial factors in replicating the local microenvironments. Recent advances in the design of BTE scaffolds have enhanced in vivo scaffold-tissue interactions. Table S1, Supporting Information, also shows that using multiple materials for fabricating these scaffolds is essential to simultaneously address both physical and chemical attributes necessary for an effective BTE scaffold.

2.2. Bone Healing Response

Bone healing is a complex regenerative process that relies on a cascade of events triggered by the body in response to the trauma. The cascade of events leading up to the formation of bone can be broadly divided into 1) an inflammatory phase, 2) a repair phase, and 3) a remodeling phase as described in **Figure 2**I.[27] Osteoblasts and osteoclasts formed as a response to this trauma are responsible for the propagation and termination of the bone healing response.

The inflammatory response is activated immediately after the trauma. It enables the recruitment of inflammatory cells and pro-inflammatory cytokines (IL-1, IL-6, TNF-α, Chemokine ligand 2 [CCL2], and others) that assist in intercellular communication necessary for the initiation of bone healing.[6,25] Previous studies have shown that, during this phase of bone healing, macrophages (M1 and M2) play a crucial role in recruiting inflammatory cells, as well as upregulating the expression of bone markers, such as Osteocalcin and Osteopontin, in MSCs.[26] The MSCs differentiate into osteoblasts and osteocytes replace damaged tissue, as shown in Figure 2III. The pro-inflammatory M1 phenotype macrophages remain at the injured site for up to 4 days before transitioning into anti-inflammatory M2 phenotypes and reducing the inflammation at the injured site.[27] Simultaneously,

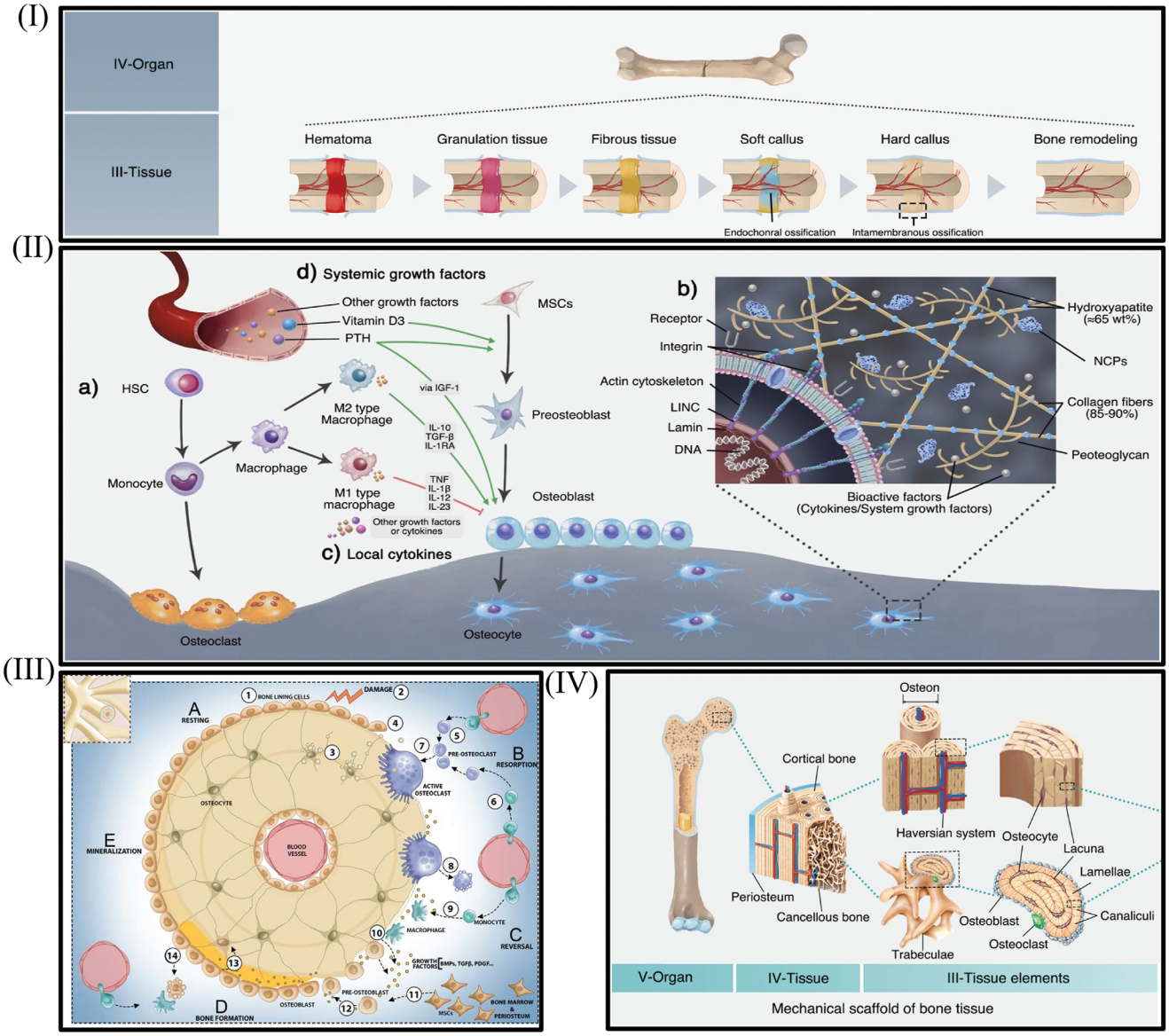

Figure 2. I) Bone healing can be broadly divided into three processes; inflammation, repair, and remodeling. The actual repair process can be broken down into five steps. These steps include hematoma formation, granular tissue formation, fibrous tissue formation, formation to soft callus, and formation of hard callus. The formation of a hard callus at the fracture site marks the termination of the bone healing step and begins the remodeling process. Reproduced with permission.[29] Copyright 2021, Elsevier. II) Cascade of cellular interaction between the monocytes and the MSCs through growth factors and cytokines leads to differentiation of MSCs responsible for the bone healing response. Reproduced with permission.[29] Copyright 2021, Elsevier. III) As shown, the process of bone formation is described in several stages (A–E). A) In response to tissue damage, osteocytes undergo apoptosis, and bone lining cells detach from their surface and initiate resorption. B) Active osteoclasts promote the mineralization of bone tissue and the resorption of broken bone fragments. Once resorption is complete, the osteoclasts undergo apoptosis. C) Macrophages differentiated from monocytes along with other growth factors ad cytokines initiate the differentiation of MSCs to osteoblasts. D) Osteoblasts produce a non-mineralized matrix and transform into osteocytes after being fully surrounded by mineralized bone tissue. E) Matrix deposited by the osteoblasts undergoes mineralization, and surface osteoblasts remain as bone lining cells. Reproduced with permission.[37] Copyright 2016, Revotech Press. IV) Location of multiple tissue elements of cancellous and cortical bone. Reproduced with permission.[29] Copyright 2021, Elsevier.

osteoclasts in the vicinity of the fracture site resorb the bone fragments maintaining the net bone mass as shown in Figure 2IIIB. Since the precise nature of the intercellular interactions between the macrophages and the osteoclasts are still unknown, it is unclear whether the macrophages directly or indirectly regulate this crucial step of bone resorption.

The repair or regeneration phase begins when the inflammation at the injured sites begins to reduce, indicating the increased presence of M2 phenotype macrophages. The M2 macrophages introduce growth factors such as IL-10, transforming growth factor-beta (TGF-β), and interleukin -1 receptor antagonist (IL-1Ra) to initiate a bone healing response (as shown

in Figure 2II).[28] Osteoblasts at this stage stimulate bone formation through intramembranous ossification and endochondral ossification.[29] Endochondral ossification involves the conversion of secreted collagen fibers into a soft woven callus. The soft callus gradually undergoes mineralization through a process of hypertrophic differentiation, causing the cartilage-to-bone transition.[29]

On the other hand, intramembranous ossification causes the direct conversion of secreted collagen fibers into a hard callus. However, to complete the repair phase, the fractured ends must be integrated with the implanted scaffold (osseointegration). Any misalignment can lead to fracture non-unions and subsequently lead to re-fractures. Eventually, the osteoblasts are completely covered with a mineralized matrix as shown in Figure 2IV, and are termed as osteocytes.[29,30] Presence of these osteocytes is critical for long-term bone remodeling or functional adaptation of bone in response to specific mechanical stimuli.[31]

The remodeling phase during the bone healing process represents the balance between osteoblastic and osteoclastic activity. The osteocytes described previously function as mechanical transducers that convert mechanical stimuli during the loading of the bone to initiate the remodeling processes.[31] Activation of the bone healing process allows the osteoclasts to migrate to a particular site and begin the process of bone resorption. This process usually lasts up to 2–4 weeks, after which the osteoclasts undergo apoptosis ceasing the process of bone resorption.[29,32] Cavities formed because of resorption then function as sites of new bone formation. Osteoblasts, monocytes, and pre-osteoblasts present in these cavities assist in forming the new bone matrix, similar to the process described in the repair phase.[32,33] The remodeling process is also a physiological process that generally occurs with age, as well as a response to metabolic activity. While the healing mechanism remains the same for both cortical and trabecular bone, differences lie in their respective bone balance (amount of bone formed minus amount of bone resorbed).[32] Bone balance in cortical bones is slightly positive, whereas it is negative in trabecular bone. Therefore, progressive loss of trabecular-type bone with age, metabolic activities, and mechanical stimuli can lead to unique structural outcomes in different patients.

The above-mentioned processes (inflammatory response, repair, and remodeling) can only occur due to the presence of the ECM. The ECM has a unique composition based on the tissue type, bone tissues generally consist of an ECM containing 40% of organic (type 1 collagen, non-collagenous proteins) and 60% of inorganic compounds (calcium deficient apatite and other trace elements), respectively.[34] However, this composition generally varies based on sex, gender, and health conditions. In bone tissues, the primary source of ECM is osteoblast cells prior to mineralization. Bone cells within this ECM use specific glycoproteins (osteonectin, thrombospondins, R-spondins, small integrin-binding ligand N-linked Glycoproteins [SIBLINGS], TGF-β) to enable functions such as bone remodeling, differentiation (of MSCs), and maintaining bone mass.[34] The collagen present in the ECM provides a matrix for the osteoblast cells to be deposited, which on the further deposition of cells forms structured bone tissues.[35] Bone remodeling is also a crucial process in addition to bone formation, and these functions are performed by osteoclasts present in the bone tissue. Changes in the stiffness of the ECM surrounding osteoclast cells regulate the expression of dentin matrix protein-1 (DMP1), which affects osteoclast attachment allowing the commencement of remodeling.[36] Therefore, mechanical stimuli are sensed by the osteocytes through glycoproteins, such as DMP1, present in the ECM.

3. Biomaterials for Bone Tissue Engineering

Metals, ceramics, and polymer classes of materials individually offer unique properties necessary for initiating and sustaining bone healing processes.[8] However, bone healing processes require materials that enable the adsorption of specific proteins, interact with the local ECM through the exchange of ions, and attract specific biomolecules or growth factors. Based on the type of interaction, materials used for manufacturing scaffolds can be classified into three types, bioinert, bioactive, and biomimetic, as shown in **Figure 3**I. Their differences in interactions from a material perspective can be narrowed down to surface chemistry, roughness, solubility, and crystallinity.

Interactions with ECM primarily occur after protein adsorption has occurred, and the nature of proteins adsorbed onto the material surface will determine the physiological response initiated by the body.[4] Positive interaction with the host tissue will enable the bone healing cascade to progress, as described previously in Section 2.2. The release of the ions can initiate the release of growth factors VEGF and BMPs, as shown in Figure 3II. On the other side, unsuitable materials initiate a foreign body response where fibrin is preferentially adsorbed onto the implant's surface. This specificity in adsorption could be due to surface charge, wettability, chemical composition, and protein structure.[4] As previously mentioned, neutrophils present in the local area of the implant attract monocytes to the fibrin-dominated implant surface. The monocytes recruited undergo differentiation into macrophages (type M1), releasing pro-inflammatory factors such as TNFα, IL-6, and IL-8. These macrophage populations at the injury site encapsulate the surface with fibrous tissue, as shown in Figure 3III.[3]

Some commonly used materials used in BTE scaffolds are shown in **Table 1**. This section will discuss the cellular interactions occurring while materials are in contact with the local ECM.

3.1. Ceramics

Ceramics have been used in biomedical applications primarily due to their inertness, hardness, and abrasion resistance.[39] For example, 3Y-ZrO_2 has been extensively used in dental crowns and bridges due to its inert nature and mechanical and tribological behavior.[40] Femoral heads of hip replacement joints, which were previously made from metals, are being replaced by ceramics (alumina, zirconia, zirconia toughened alumina, or silicon nitride) due to their superior tribological properties and wear resistance.[41] These ceramics discussed here are fully capable of satisfying the mechanical requirements of the above-described applications, however, their inert nature prevents any interaction with the body.

The only ceramics capable of interacting with the body include bioglasses (BGs) and calcium phosphate-based ceramics.

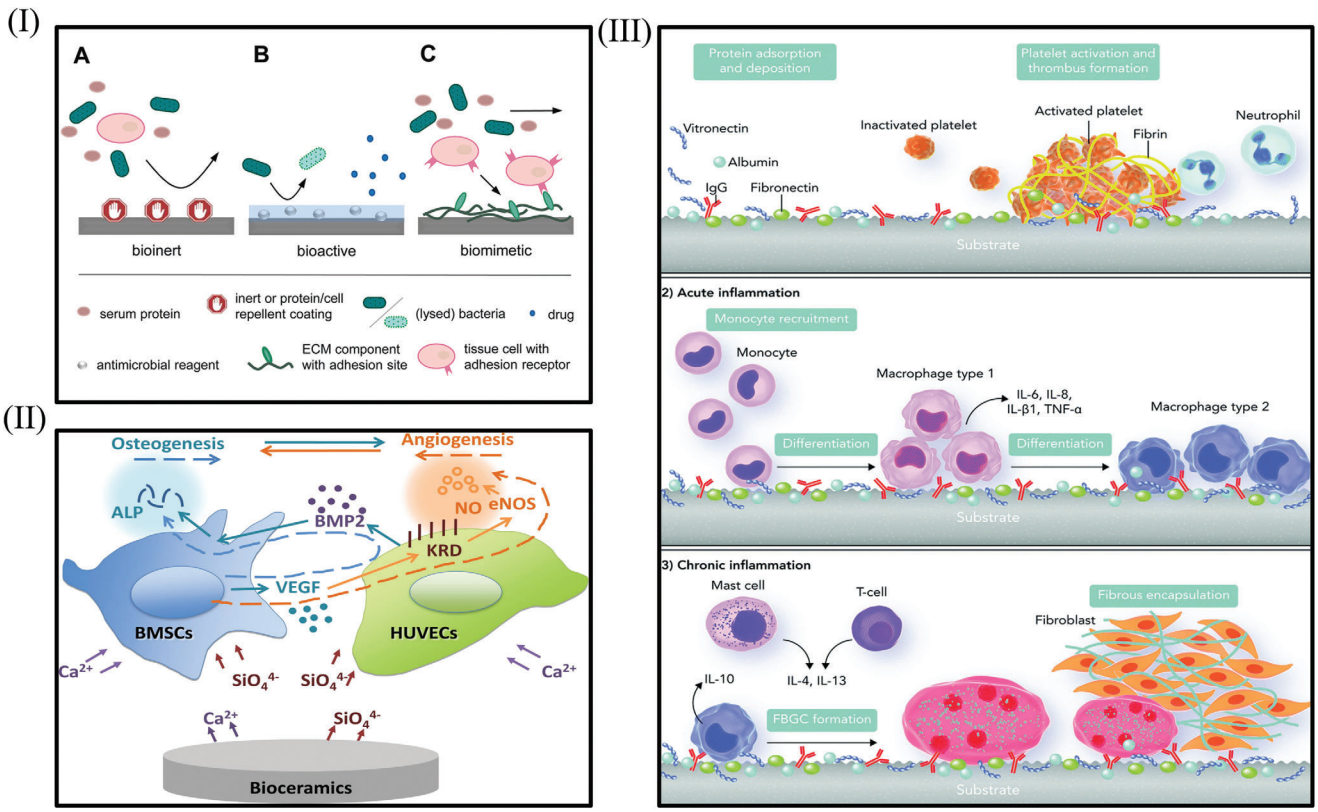

Figure 3. I) Materials based on the nature of interaction can be classified into bioinert, bioactive, and biomimetic. Bioinert materials repel or do not interact with ECM proteins. When implanted inside the body, bioactive materials can release biomolecules, enabling interaction with ECM through biomolecule uptake. Biomimetic surfaces can mimic naturally found tissues in the body, allowing cellular interactions through surface-bound ECM proteins. Reproduced with permissio.[4] Copyright 2021, De Gruyter. II) The exchange of ions at the interface of bioceramic–ECM initiates osteogenesis and angiogenesis at the implanted site. Mesenchymal stem cells present in the ECM undergo specific differentiation into osteoblasts and osteocytes in the presence of specific biomolecules. Osteoblasts initiate bone formation leading to an upregulation of alkaline phosphatase (ALP) activity. Osteoclasts regulate bone formation and assist in their constant remodeling.[38] Reproduced with permission.[38] Copyright 2019, Elsevier. III) Foreign body response to implanted material, as shown here, occurs in three stages involving 1) non-specific protein adsorption, 2) monocytes recruited at the local site induce inflammation, and differentiate into type 2 macrophages, 3) Type 2 macrophages along with T cells and Mast cells increase the number of foreign body giant cells. Fibroblasts recruited by the FBGCs cause collagen deposition around the implant surface, forming a thick fibrous layer. Reproduced with permission.[3] Copyright 2020, the Royal Society of Chemistry.

Table 1. Biomaterials commonly used for bone tissue engineering applications.

Material type	Materials
Ceramics	Calcium phosphate ceramics (HAp, α-TCP, β-TCP, and BCP), ZrO_2, and black akermanite (Ca_2MgSiO_7)
Polymer	Polylactic acid (PLA), polyurethanes, polyethylene glycol (PEG), polyglycolid (PGA) and poly caprolactone (PCL), polyether ether ketone (PEEK), collagen, chitosan, alginate, and hyaluronic acid
Metals	Stainless steel, titanium alloy (Ti6Al4V), tantalum, magnesium, and cobalt-chromium alloys
Bioglass	Acidic oxide bioglasses and basic oxide bioglasses, 45S5 bioglass, and borate-based bioglasses (BBG)

Bioglasses are synthetic vitreous materials chemically similar to natural bone minerals. They are known to undergo rapid degradation forming HAp on their surface, leading to biological fixation.[42] More recent studies have identified techniques to tailor these degradation rates to the growth of the tissue.[43] While they are superior to phosphate-based ceramics in their ability to interact with the body, they lack the mechanical properties to provide support, making them unsuitable to be used on their own.[43] Calcium phosphate ceramics (CPCs) used for BTE scaffolds are known to be osteoinductive and osteoconductive. The bone healing effect of the CPCs is strongly dependent on the Ca/P ratios, crystallinity, and composition. CPCs with a Ca/P ratio of 1.5 are highly soluble in aqueous environments causing the release of Ca^{2+} and PO_4^{3-} ions, so a carbonated apatite layer forms over the surface. CPCs, such as hydroxyapatite, possess a stoichiometric ratio of 1.67, making them more stable, and therefore, less soluble in the aqueous environment of the body.[8] Therefore, bioceramics enable protein adsorption and communication with the local ECM through a solution-driven and cell-mediated process. While the exact nature of this communication with the ECM is still unknown, the process is highly dependent on the type of proteins adsorbed onto the surface of the ceramic.[3] Therefore, to modify this property, CPCs are doped with cationic or anionic impurities to alter their dissolution rate and stability or improve

Table 2. Effects of cationic and anionic dopants in CPCs on their cellular interactions.

Calcium phosphate ceramic	Dopants	Biomedical properties	Ref.
BCP	Cu	• Controlled release of Cu^{2+} ions • The release of Cu^{2+} ions introduced an anti-microbial effect • Cu^{2+} increased angiogenesis at the injured site by enhancing the hypoxia-like tissue reaction	[44]
BCP	Mg	• Increased rate of apatite formation in the presence of Mg^{2+} ions • Mg^{2+} ions upregulate Fibroblast growth factor (FGF23) through elevation in Runx2, osteocalcin, and osterix expression. • Higher integrin receptor affinity to Mg^{2+} ions improved cell adhesion to the doped microscaffold • Collagen secretion and ALP activity were absent	[45]
β-TCP	Mn	• Increase in protein adsorption capacity • Increase in expression of ALP, Runx2, type 1 collagen, and osteocalcin • Optimal concentration of Mn^{2+} ions must remain below 7.17 μg L^{-1} to observe improvement in mBMSC proliferation and promote early-stage differentiation • Mn^{2+} and Mn^{3+} ions are responsible to limit the accumulation of ROS[a)] species at the inured site	[46]
HAp	Sr	• Higher expression of Type 1 collagen and BMP compared to pure HAp • Could be toxic to the cell at high concentrations • Increased formation of bone compared to HAp • Inhibited osteoclast activity thereby producing increased bone formation	[47]
HAp	CaF_2	• Enabled rapid formation of apatite layer when soaked in simulated body fluids • Showed good stability in the Ca/P ratio after immersion in SBF fluids • Micropore formation due to the dissolution of F-HA coating enhanced osteogenesis and ion exchange • ALP activity showed a significant increase at the early stages of soaking	[48]

[a)] The role of reactive oxygen species (ROS) is still an active area of research, and therefore, future research will determine their necessity in bone healing pathway; Note: biphasic calcium phosphates (BCP); tri-calcium phosphate (TCP); hydroxyapatite (HAP); Ostoegenic-related transcription factor (osterix).

biological functionality. **Table 2** shows how the functionality of certain CPCs has been improved by doping.

The low mechanical strength and brittle nature of CPCs still make them unsuitable for use in load-bearing areas.[49] To enhance their structural strength, they are used in combination with polymers, metals, and other ceramics, which are termed multi-material scaffolds. Incorporation of more than one material can be achieved in several ways such as homogenous mixtures, polymer matrix composites, coatings, ceramic matrix composites, and in the form of layers.

3.2. Polymers

Polymers used for BTE can be further classified into natural or synthetic, based on their source. As shown in Table 1, alginate, chitosan and collagen are natural polymers that are used for BTE applications. Natural polymers tend to elicit a positive response during ECM interactions due to their ability to easily bind proteins to their surfaces and their similarity with tissues found naturally in the body.[50] For example, type 1 collagen is a constituent of bone, as described in previous Section 2.2. However, its low structural strength, difficulties in processing samples, and the potential risk of disease transmission restrict its usage in BTE applications.[51] Synthetic polymers, such as polylactic acid (PLA), polycaprolactone (PCL), polyglycolic acid (PGA), and polyurethane (PU) can address the above limitations of natural polymers as the hydrophobic nature of these polymers prevents protein adsorption and requires direct interactions with ECM to induce a bone healing response.[52] Therefore, polymers are often functionalized with natural proteins or peptides, such as RGD, YIGSR, and IKVAV, to enhance cell attachment and proliferation.[2]

Polymers, such as PLA, PGA, and PCL, undergo degradation through hydrolysis of the ester linkage, lasting anywhere between a few months to years depending on the polymer's crystallinity, composition, and hydrophilicity. Degradation times of 3–6 years, 1–2 years, and 3–4 months are typically observed for PLA, PCL, and PGA, respectively.[53] Degradation of the polymer occurs when the scaffold is in contact with ECM causing physiological and mechanical changes to the implanted scaffold. For example, hydrolysis of PGA leads to increasing local pH slowing down the process of osteogenesis.[54] In addition to hydrolysis of the polymer, proteins, biomolecules, growth factors, and peptides bound to the polymer surface are critical to initiate a bone healing cascade.[55] **Table 3** highlights the effects of using secondary phases/polymers to functionalize polymer scaffolds. Further, these bioactive polymers can be used as carriers of growth factors and biomolecules to aid bone healing.[56] Polymer scaffolds can be biologically effective as BTE scaffolds; however, the insufficient mechanical strength of polymers, along with increasing porosity, make them unsuitable for use in load-bearing areas.[8]

3.3. Metals and Alloys

Metals commonly used for BTE are bioinert, that is, they do not initiate a foreign body response when implanted.[8] These metals and alloys include titanium alloys, tantalum alloys,

Table 3. Function of secondary phases used along with polymer composite scaffold and its implications on their cellular interactions.

Primary polymer	Secondary polymer/phase	Biomedical property	Ref.
PCL	Bioglass and GelMA	• Enhanced hydrophilicity of PCL scaffold • Reduction of contact angle to less than 40° • Increased protein adsorption • The release of Na, Si, and Ca ions present in bioglasses assist in mineralization and initiating the bone healing cascade • Negative surface charges increased the rate of bone mineralization	[55]
Citric acid-based polymer	HAp	• Upregulation of ALP activity and Osterix gene expression • Citrate molecules assist in bridging mineral platelets improving bone crystallinity (improving bone strength).	[57]
PLA	Polydopamine (PDA) and type 1 collagen	• Up to 92% increase in type 1 collagen immobilization on the polymer surface • Increased cell proliferation after 7 days of culture • The presence of PDA enhanced metabolic activity • 3D infiltration of ECM was achieved due to covalent immobilization of ECM proteins • Presence of PDA enables the covalent immobilization of biomolecules such as BMP-2, VEGF, and RunX2	[58]
PCL	Gelatin, bacterial cellulose, and HAp	• Increased proliferation and attachment due to the inclusion of natural polymers	[59]
Chitosan	AgNP	• Chelation with silver ions improved the degradation rate of chitosan • An antibacterial effect was observed due to the presence of silver nanoparticles • Upregulation of RunX2 and increased Alp activity	[60]
PLGA	TiO_2	• Increased mechanical strength • Increased protein adsorption • TiO_2 nanoparticles aid in the precipitation of bone-like apatite • In-process formation of calcium titanate leads to high osteoblast adhesion • Increased attachment sites for binding bioactive receptors • The presence of TiO_2 leads to accelerated hydrolytic degradation	[61]
PVA and chitosan	Carbonated Hap (CHAp)	• The occurrence of carbonated HAp nanoparticles was identical to that of natural bone • Reduced polymer crystallinity due to the presence of amorphous interfaces • The increase in mechanical strength was less than 30% • Reduced elongation due to accumulation of HAp nanoparticles on polymer fiber • The presence of CHAp increases the number of favorable sites for the protein adsorption • Interaction of Ca^{2+} and PO_4^{3-} ions leads to bone mineralization	[62]
PVDF	Graphene oxide	• Increased mechanical performance due to graphene oxide reinforcement • Increase in hydrophilicity due presence of hydroxyl functional groups • Electro-mechanical stimulation of scaffolds showed upregulation in ALP activity	[63]

magnesium alloys, and zinc. The use of these metals and alloys for BTE application could be in the form of bulk materials, nanoparticles, or both. Functionalities observed based on the distinction in their form are vastly different.[8,64] However, the critical issue in the utilization of metal alloys in their bulk material form is the mismatch in mechanical properties with natural bone. The mismatch in load-bearing capacities can cause resorption of bone in the surrounding areas of the implant leading to loosening or complete failure in attachment.[8,30] Further, the bioinert nature of some metals and alloys in bulk and nanoparticle form limits their ability to interact positively with the local ECM and initiate a bone healing response.[64,65]

Titanium alloys are commonly used for orthopedic applications primarily due to their bioinert qualities.[65] To functionalize these metal alloys for BTE applications, alloying elements, such as Zr, Nb, Al, and V, are added to improve the interaction with the local niche and improve corrosion behavior.[66] Previous studies utilizing Nb and Zr additions to Ti alloys have shown increased alkaline phosphatase (ALP) activity and reduced cytotoxicity.[66,67]

Bioresorbable metals, such as Zn, Fe, and Mg, are recently becoming more popular for BTE applications. Zn has recently been a popular material for usage in BTE applications because of its nominal degradation rate and the importance of Zn finger proteins (ZFPs) in the human body as DNA-binding transcription factors responsible for the regulation of numerous cellular processes.[68] Zn, when implanted, undergoes degradation due to galvanic coupling, releasing Zn ions which further interact with Ca^{2+} and PO_4^{3-} ions present in the simulated body fluids (SBF).[68] However, the uptake of Zn ions within the body is limited to about 15–40 mg day^{-1}.[68,69] Therefore, degradation of the scaffold needs to be adjusted to not exceed this physiological limit.

Magnesium, like Zn, is bioresorbable in nature and the major difference lies in the degradation rate. Degradation of Mg within the body occurs rapidly, leading to a release of hydrogen gas (H_2).[70] The release of H_2 gas was shown to interrupt the bone healing cascade due to the increase in the local pH of the surrounding area.[71] Even with these limitations, Mg is used as

a prospective material for bone replacement due to the similarity of its mechanical strength to that of bone and the importance of Mg ions for physiological functions within the body.[70]

Nanoparticles used along with other bioactive materials can impart osteogenic or other properties necessary to initiate and sustain the bone healing cascade.[64] The most commonly used nanoparticles include gold (AuNP), silver (AgNP), iron, aluminum, copper, zirconium, and hydroxyapatite nanoparticles.[64] Low dosages of AuNP have been shown to function as synthetic replacements for bone morphogenic proteins (BMP), that are directly responsible for regulating bone mass through Wnt/β-Catenin signaling pathways.[72] Silver nanoparticles are known for their bactericidal effects, being able to penetrate the bacterial cell wall, and damage their DNA.[64] Titanium oxide nanoparticles are commonly used in BTE applications through addition into polymer scaffolds. The addition of these nanoparticles has been shown to improve the wettability and mechanical properties of the resultant polymer scaffold.[61]

3.4. Multi-Material Scaffolds

Multi-material scaffolds involve using two or more materials in the form of homogenous mixtures, discrete structures, doping agents, or surface coatings. Depending on the nature of the combination, the properties of the composite can be significantly different. For example, nano-HAp, when homogeneously mixed with zirconia-based scaffolds, can function first as a bioactive site and second, improve mechanical strength by delaying crack propagation.[73] Scaffolds with nano-HAp coatings on Ti alloys enable interaction with the ECM to improve osseointegration but do not contribute to the strength of the material due to its weak surface adhesion.[74] BG, as previously described, is highly bioactive and could assist in early osteointegration. As a result, BG coatings are applied on stainless steel, Ti-6Al-7Nb, nitinol, and other biocompatible alloys.[75] Multi-material scaffolds have more recently seen application as drug delivery devices, which has become possible with the combination of organic and inorganic biomaterials. Chitosan-HAp-based scaffolds have been shown to function as therapeutic metal ion delivery vehicles of strontium and copper ions. The strontium-substituted HAp functioned as a source of Sr ions, which are known to enhance bone formation and influence gene expression of osteoclasts.[76] The chitosan polysaccharide, being the carrier of copper ions, inhibited the replication of bacteria due to the initial burst release of Cu ions.[76,77] The inclusion of natural polymers in bioceramic scaffolds is still a challenge due to the high post-processing temperatures required to increase the mechanical strength of ceramic materials. The inclusion of starch-based natural polymers into HAp-PCL-based composites has been shown to improve mechanical properties by functioning as a binder.[78] Further, the presence of starch increased the degradation time of these scaffolds. Preventing increased surface degradation allows cellular growth and adhesion, which are essential in BTE scaffolds.[78] Materials used on their own are more likely to be unsuitable for BTE applications due to their inherent limitations, thus, combining them to form composites can help overcome the limitation described above. Therefore, recent studies have explored multi-material scaffolds for BTE applications.[79]

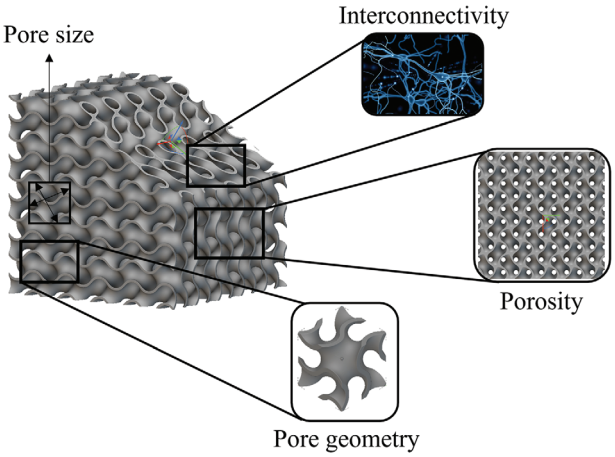

Figure 4. Description of the features of a porous scaffold used for bone tissue engineering. Pore sizes refer to the diameter/dimension of the pore. Porosity of the scaffold refers to the ratio of the total pore volume to the volume of the scaffold. Pore geometry refers to the arrangement of pores within the scaffold. Interconnectivity of the scaffold refers to the number of paths connecting the pores present in the scaffold.

Including a secondary phase in the form of nanoparticles, doping agents, or uniform mixtures can influence the composite's chemical nature; the processing methods of composites are also known to have similar effects. For example, processing magnesium alloys containing nano-BG particles using the powder metallurgy technique has been shown to introduce intermetallic Mg_2Si and MgO phases that lead to rapid in vitro degradation of the magnesium-based composite.[80] However, processing the same composite using spark plasma sintering (SPS) prevented the formation of intermetallic phases, and the retention of nano-BG within the matrix of the magnesium alloy reduced in vitro degradation and improved cell viability.[81] Therefore, simultaneously processing these materials will pose challenges in creating multi-material scaffolds.

4. Scaffold Structure

The porous architecture of BTE scaffolds is characterized by four factors: 1) porosity (%), 2) pore size, 3) surface area, and 4) interconnectivity as shown in **Figure 4**. Porosity refers to the volume percentage of free space present within the scaffold architecture. Pore sizes refer to the average dimensions of the pores present in the scaffold. The surface area of the scaffold is a function of pore sizes present on the surface and porosity of the scaffold. The interconnectivity of the scaffold is a function of the spatial location of the pores, their sizes, and porosity and determines the extent of cell infiltration and nutrient transport achievable when the scaffold is implanted inside the body.

4.1. Pore Size

The pore size of the scaffold is a critical parameter that determines the extent of infiltration achievable and its mechanical strength. **Figure 5**A shows that increasing pore size is inversely proportional to the compression strength of these porous scaffolds, and therefore, pore size must be carefully chosen to allow

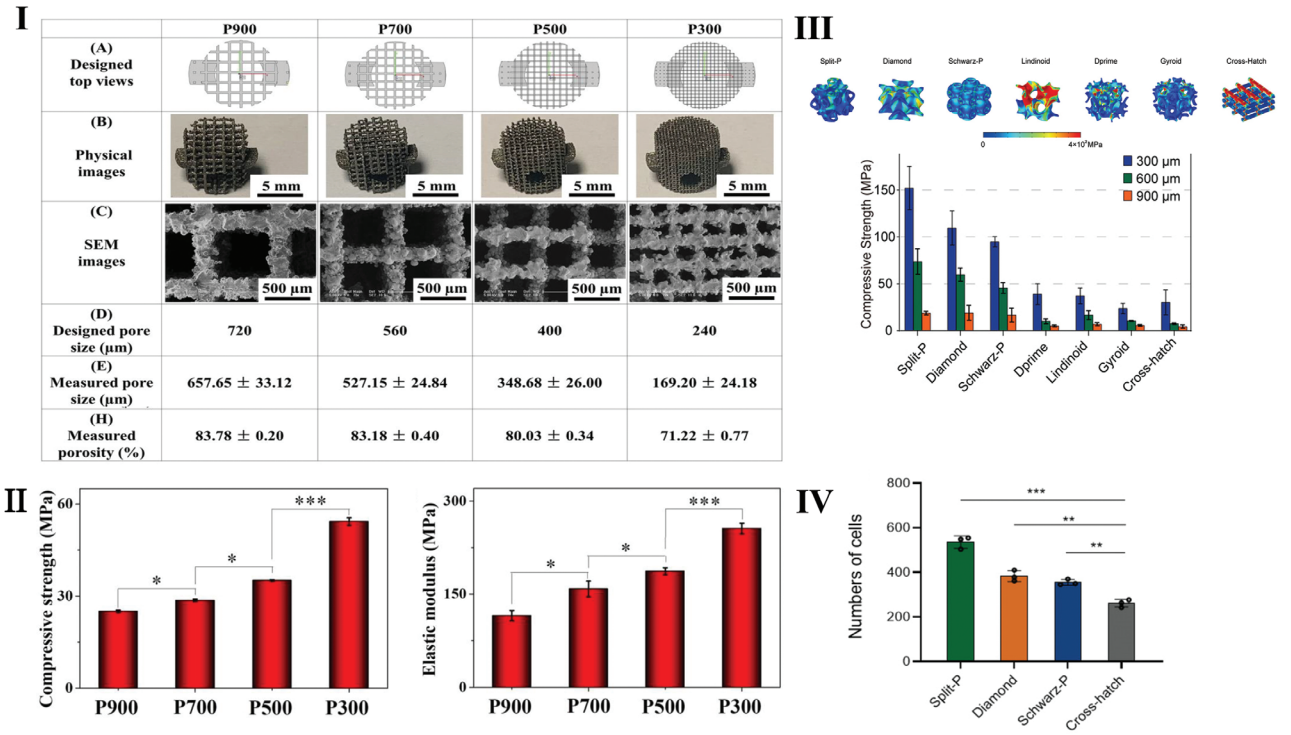

Figure 5. I) Cylindrical Ti-6Al-4V scaffolds fabricated using selective laser melting (SLM) at four different pore sizes and struct thickness values. Reproduced with permission.[100] Copyright 2021, Elsevier. II) Increasing pore sizes from P300 to P500 shows a significant reduction in compression strength. Compression strength of P500, P700, and P900 scaffolds remained similar. There was a gradual decrease in elastic modulus with increasing pore sizes. Reproduced with permission.[100] Copyright 2021, Elsevier. III) Pore geometries (gyroid, split-P, diamond, schwarz-p, lindinoid D-prime, cross-hatch) showed varying stress distributions when loaded. The split-P, diamond, and schwarz-P structures showed low-stress concentration while the lindinoid and cross-hatch structures showed high-stress concentration on the scaffold surface. Split-P structure showed the highest compression across all pore size ranges (300, 600, and 900 μm) while the cross-hatch and gyroid structure showed the lowest compression strengths at all pore sizes Reproduced with permission.[101] Copyright 2022, Wiley-VCH GmbH. IV) The interconnected nature of TPMS structures allowed for increased cell migration throughout the porous volume which is reflected in its higher cell density compared to the cross-hatch structure. Reproduced with permission.[101] Copyright 2022, Wiley-VCH GmbH.

for fluid ingress and provide strength. Pore sizes commonly used in BTE scaffolds vary between 100 and 900 μm.[82] Osteoblast cells (10–50 μm in size) prefer pore sizes greater than 300 μm as this enables infiltration of biomolecules and transportation of nutrients and waste.[79,83] Increasing pore sizes have also been shown to reduce the water contact angle, enabling higher fluid ingress when implanted within the body.[84]

Bone in-growth within the scaffold during the healing process is critical to ensure load transmission and fixation of the scaffold to the natural bone. Smaller pore sizes (200–300 μm) and limited space for infiltration are known to induce chondrogenesis of the MSCs leading to the formation of cartilaginous tissues as opposed to bone tissue.[85]

Optimal pore sizes for in-growth have been shown to be within the range of 250–500 μm.[8,86] The inclusion of large pores, while beneficial for functionalizing the scaffold, can reduce the strength of the scaffold affecting its structural capacity.[87] However, smaller pores (≤100 μm) cause fibrous tissue formation around the scaffold, which physically prevents angiogenesis and any interaction with the scaffold surface.[79] Previous studies have shown that micropores (within 10 μm) increase the available surface area, promoting ion exchange and bone protein adsorption.[88] These results indicate that different pore sizes impart unique physiological and structural properties to BTE scaffolds. Thus, heterogeneity in pore sizes can simultaneously enable multiple features critical for bone healing.[89]

4.2. Porosity

The porosity of the BTE scaffold is a function of the pore size and geometry of the scaffold, when implanted the porous volume of the scaffold houses osteoblasts cells and functions as a site for cellular interaction. Scaffolds used for BTE application have porosities ranging from 50% to 80%, depending on the required mechanical performance. Higher porosities (greater than 65%) allow greater infiltration of ECM but reduce the structural capacity of the scaffold as shown in Figure 5.[90] Higher scaffold porosities provide larger surface areas ensuring greater interaction with the ECM.[91] This promotes faster degradation or bone ingrowth and assists in vascularization.[85] Further, continuous contact with ECM will lead to pore occlusion over time, therefore, larger porosities present in the scaffold will ensure sufficient permeability for the transport of nutrients and biomolecules. Porosities below 65% provide higher mechanical strength while reducing the ability to interact with the ECM. The reduced ECM

interaction and lack of cell spreading reduce the ALP activity of the cells.

Permeability is a critical requirement, which is influenced by the porosity and interconnectivity of the porous scaffold. The required extent of permeability will depend on the size of the defect, larger defects require a greater supply of oxygen and nutrients for the process of bone healing to proceed.[92] For example, cell proliferation studies performed on a 3D-printed stainless steel scaffold with a porosity of 58% showed higher cell proliferation and growth compared with scaffolds with 60% and 70% porosity. The higher cell proliferation and growth at the lower porosity was due to its ability to retain the cell media for longer compared to scaffolds with 60% and 70% porosity.[93] Therefore, the nature of porosity can also influence bone healing behavior. A highly open porous scaffold, while good for promoting angiogenesis, can have a reduced ability to promote cell growth and proliferation.

4.3. Scaffold Geometry

Scaffold geometry refers to the arrangement of pores within the scaffold matrix. The scaffold geometry observed in BTE scaffolds can be classified into two types based on the orientation of their structure as randomized and regular. Randomized orientation refers to scaffolds that lack any repeating units. While these structures tend to mimic the natural bone morphology,[94] their random orientations create inconsistencies in scaffold compression strength and are extremely difficult to replicate.[95] Scaffolds with regular orientations include cubic, hexagonal, triply periodic minimum surfaces (TPMS), spherical, and honeycomb arrangements. While these structures are not directly responsible for bone healing, their ability to ensure vascular growth, nutrient diffusion, and load-bearing ability make them an ideal choice.[96] TPMS structures have recently become a popular choice for use in BTE scaffolds because of their ability to ensure the ideal combination of stiffness and permeability.[97] Yanez et al.[98] showed that gyroid-based scaffolds used for bone defect reconstruction showed compression strengths within the range of human trabecular bone (1.5–45 MPa) at porosities of 75% and 90%. Further, the layer-by-layer collapse of the scaffolds and the elliptical strut shape oriented in the direction of load provided a high stiffness and strength to the scaffold. It also indicated the significant differences in plastic deformation at 45° loads when compared to axial loading.[98] Thus, load direction must also be considered when selecting scaffold geometry. Since the effect of pore geometry on bone healing response is a function of porosity, pore sizes, interconnectivity, and surface area, isolating the effects of pore geometry can be challenging. However, its influence on mechanical properties can be clearly isolated as shown in previous studies,[99] hence the most common approach involves analyzing bone healing behavior based on scaffold features (pores size, porosity, and interconnectivity) while the mechanical properties are explored via the influence of pore geometry.

4.4. TPMS Structures

Minimal surfaces can be defined as surfaces with a zero mean curvature and possessing the least surface area within the bound area. When these surfaces are periodically repeated along any three axes, they are termed triply periodic minimal surfaces. The implicit functions of these structures can be defined using the trigonometric functions, unit cell length, and type of unit cell.[102] Due to this, they can be modified using the variables described in **Table 4**. The three basic types of TPMS structures include the primitive type (P-type), gyroid type (G-type), and diamond type (D-type).

Table 4. Mathematical equations describing triply periodic minimum surface structures.

TPMS structure	Equation	Ref.
Gyroid	$\cos(wx) + \cos(wy) + \cos(wz) = c$	[102, 103]
Diamond	$\sin(wx)\sin(wy)\sin(wz) + \cos(wx)\sin(wy)\sin(wz) + \sin(wx)\cos(wy)\sin(wz) + \sin(wx)\sin(wy)\cos(wz) = c$	
Primitive	$\cos(wx) + \cos(wy) + \cos(wz) = c$	

'w' represents $2\pi/l$, l represents the unit length of the unit cell, and c represents the level-set function.

Mechanical strength and energy absorption of TPMS structures have been shown to be more reliant on the type of structure rather than the material itself. P-type structures exhibited a fluctuation in stress at the plateau stage due to the localized buckling of curved walls. Failure in these uniform P-type structures initially occurred perpendicular to the applied load, which represents the first peak on the stress–strain curve while the remaining fluctuations arose from the gradual buckling of the P-type unit cell.[104] Thus, the stress–strain response can be altered by changing the geometry and thickness of the P-type unit cell structure.

Gyroid-type structures, having an unconnected porous structure, prevent the propagation of microcracks making them structurally stronger than the P-type TPMS structures.[104,105] Diamond-based TPMS structures have been shown to provide the highest mechanical strength when compared to P-type and G-type structures. Stress–strain response of diamond-based structures showed a significant change in plateau stress when changing from a sheet diamond to a skeletal diamond.[106] Skeletal-diamond structures undergo a single diagonal shear when applied stress exceeds peak stress, while a sheet diamond requires the formation of a double shear band for failure to occur,[107] allowing for greater energy absorption, and hence, higher toughness of the sheet-diamond structure.[106,107]

The interconnecting and non-penetrating architecture of TPMS structures is very common in biological systems due to its ability to fulfill unique requirements demanded by cellular functions.[102,108] The concave surfaces of TPMS structures promote osteogenic cell differentiation compared to scaffolds with flat or convex surfaces. For example, a HAp scaffold with a split-P architecture was shown to be more favorable in the formation of new bone compared to HAp scaffolds with the cross-hatch architecture when implanted into rabbit joints.[101] Bone growth was shown to begin at the outer surfaces of the scaffold and continue inward and the interconnected architecture of the split-P scaffold enabled the complete recovery of the rabbit femur within 12 weeks.[101] The architecture of these structures (pore size, porosity, and geometry) will influence mechanical strength, permeabil-

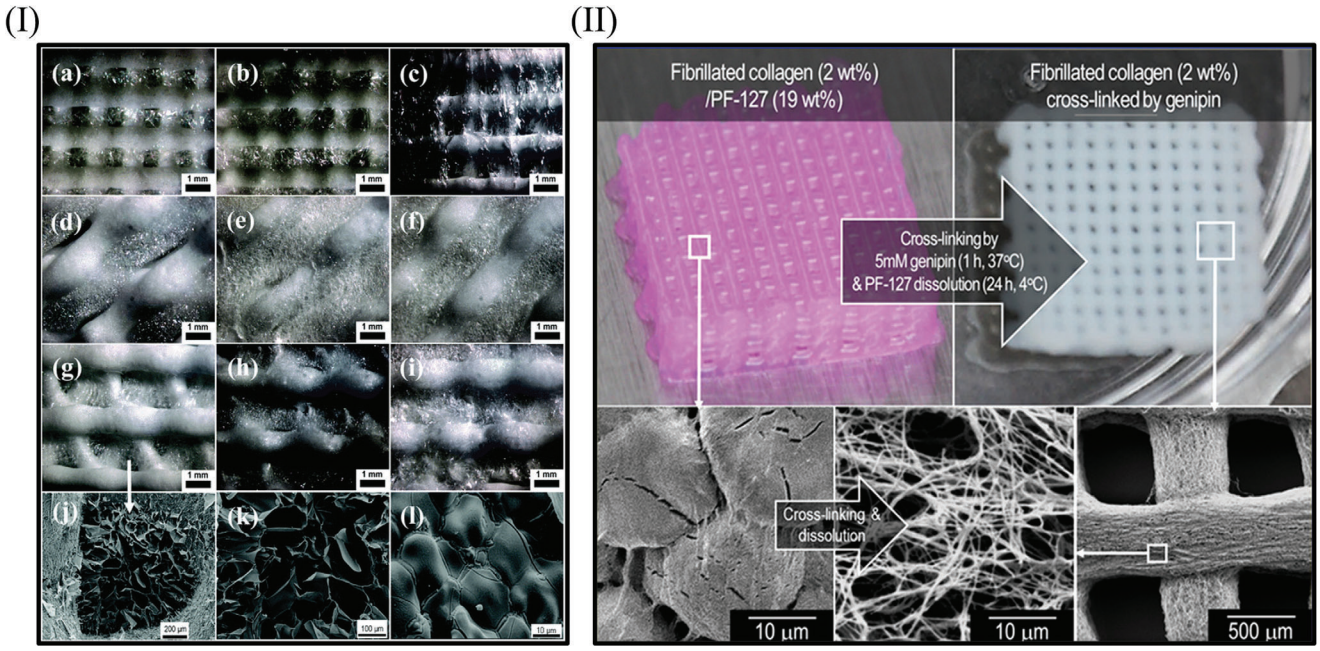

Figure 6. I) Represents the range of pore shapes (square, parallelogram, and triangles) explored for BTE application using bioceramic–silk scaffolds. Macropores (≈1mm) were introduced using 3D printing and micropores (≈50–100 μm) were produced by freeze-drying different concentrations of silk (0.625%, 1.25%, and 2.5%). Reproduced with permission.[109] Copyright 2015, the Royal Society of Chemistry. II) Fibrillated collagen scaffolds produced with the combination of pore sizes that extend from a few mm to nanometers using bioprinting and the selective leaching of PF-127 solution. Reproduced with permission.[111] Copyright 2018, American Chemical Society.

ity, and cellular growth. Similar to natural bone structures, there is a hierarchical distribution of structural features as shown previously. In order to mimic this natural environment, scaffolds need to have an ordered arrangement of features that provide the ideal combination of mechanical strength, stiffness, and permeability.

4.5. Hierarchical Structures

Hierarchical structures involve the use of a combination of pore sizes, porosities, and pore geometries. As described previously in Section 3, differences in these critical scaffold features can elicit vastly different responses during the bone healing process since bone healing involves a cascade of signaling pathways that are based on the scaffold—ECM interaction. The presence of multiple pore sizes and geometries thus become essential features for BTE scaffolds.

Xu et al.[109] showed that 3D-printed bioceramic-silk composite scaffolds showed an increase in the recruitment of BMSCs and expression of the osteogenic markers, OPN, BMP 2, and RUNX2. Cell attachment rates during the first 7 days were the highest in the prepared hierarchical scaffold. While larger pore sizes of greater than 100 μm enabled full infiltration of ECM, mesopores ranging between 50 and 100 μm at the silk fibroin prevented cell leakage from the larger pores during cell culture. In vivo studies involving the implantation of scaffolds in rabbit femur defects showed increased new bone formation.[109]

Lei et al.[110] prepared hierarchical scaffolds having pore sizes ranging from 8 nm to 5 μm, using Hydroxyapatite-doped dendritic mesoporous silica nanoparticles (HA-DMSN). The presence of these nanopores is known to be an interesting prospect for drug delivery systems involving in situ delivery of growth factors to the implanted site. In vivo bone regeneration on a rat cranial defect model using HA-DMSN scaffolds showed the largest bone formation after just 4 weeks of implantation. A primary reason for increased bone formation was an interconnected nano and microporous structure. The similarity in scaffold porosity to natural bone assisted in inducing specific functions for bone regeneration.

Lee and Kim[111] prepared a hierarchical nanofibrous collagen scaffold with varying strut thicknesses. The 3D printed structure consisted of macropores, micropores, and nano-fibrous struts introducing a hierarchy in the scaffold architecture. In vitro studies using MC3T3-E1 cells showed better protein adsorption (fibronectin, vitronectin, fibrinogen, and laminin) due to the higher surface area available on the fibrous struts. Further, this nanofibrous structure allowed for the unipolar extension of the cell cytoskeleton allowing for the extension and contraction of the cell structure. Since the cell absorption was higher in the nanofibrous scaffold and there was a lack of interconnectivity, the proliferation of cells was hindered. However, the larger pores present in the collagen-based scaffold were able to provide a significantly larger area for cell proliferation (**Figure 6**).

5. Manufacturing Hierarchical Structures for Bone Tissue Engineering

Manufacturing hierarchical porous structures require control over the size and position of the pores introduced. Conventional manufacturing techniques for the production of porous

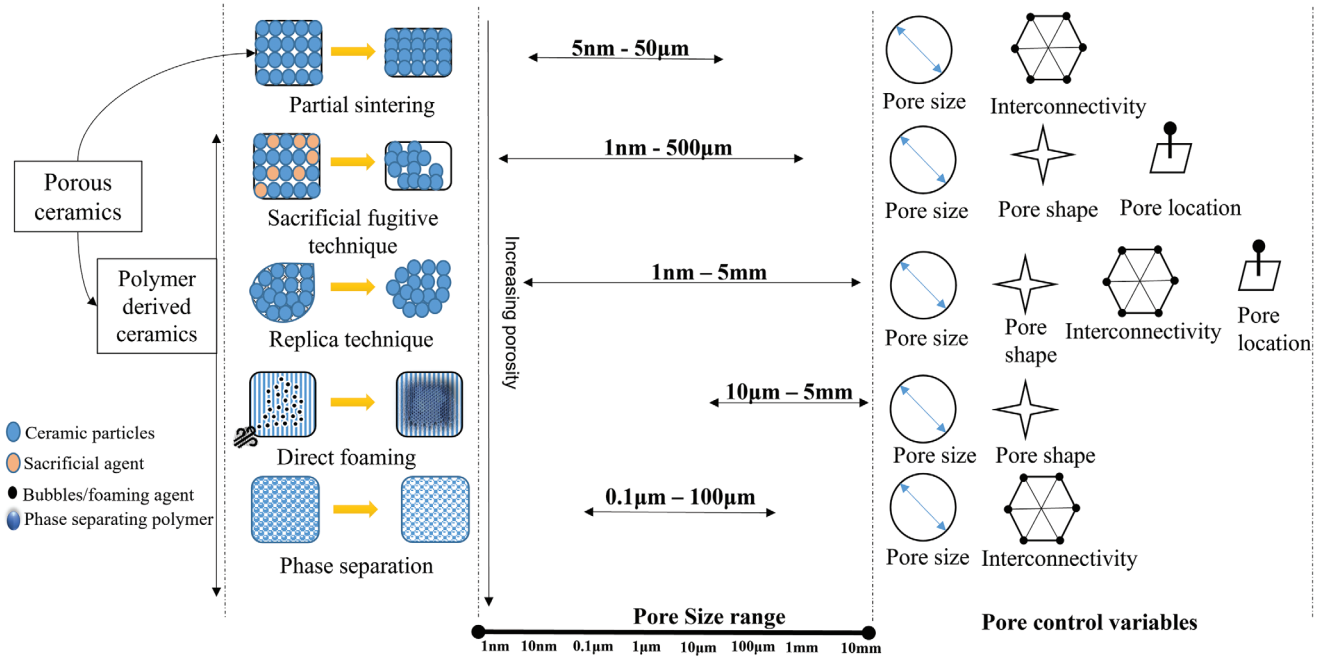

Figure 7. An overview of conventional manufacturing techniques to produce porous ceramics.

materials are briefly described in **Figure 7** and can be used to produce macro ($d > 50$ nm), meso (50 nm $> d >$ 2 nm), and micro ($d < 2$ nm) porosities.[112] Only specific techniques under these pore-forming methods can produce hierarchical porosities. These techniques include freeze casting, self-assembly, spin coating, hydration process, nano-stereolithography, and additive manufacturing.[113]

Freeze casting is a technique used to produce aligned porosities; this technique involves cooling liquid template-creating channels within the slurry in the direction of the thermal gradient. Dendrites formed during the cooling of the liquid template function as a link between the pore channels.[112] Process parameters of the freeze casting process include freezing rate, slurry formulation, and the solvent used. While freeze casting can produce a range of pore sizes, pores generated are oriented in the direction of cooling. Also achieving different pore sizes within the same structure will require careful tuning of process parameters (freezing rate, slurry viscosity, and concentration of suspension and preforming agent). Freeze casting has previously been used in the preparation of hydroxyapatite-gelatin scaffolds, producing a lamellar microstructure with pore sizes between 18 and 125 µm. The concentration of HAp and cooling rate showed a significant impact on the microstructure and morphology of the sample.[114] Lee et al.[115] produced graded porous hydroxyapatites using a sequential freeze-casting process. This was achieved by using different concentrations of HAp (10, 15, 20, 25, 40, and 50 vol%), producing a porosity between 25% and 70%. Pore sizes up to 160 µm were fabricated using this method depending on the HAp concentration, concentrations exceeding 45 vol% showed very low porosity and pore sizes due to the high viscosity of the slurry used for freeze casting.[115] However, as described in Figure 7, this technique lacks control over the spatial location of the pores and pore shape.

The principle of the replica technique involves using open-celled porous templates coated with ceramic slurry to form a defined internal pore network. This is followed by thermal heat treatment to eliminate the template through thermal decomposition.[116] Once the template is eliminated from the matrix, it is sintered to form the required porous ceramic. Porous ceramics generated using these methods have been used to prepare scaffolds for BTE[117] due to their highly reticulated nature and control over pore sizes. For example, PU foams used as templates while producing porous ceramic scaffolds need to have high porosity (>90%) with pore sizes larger than 100 µm.[118] Commonly used PU foams having pore density values ranging from 5 to 80 ppi have been shown to produce well-defined pore structures with complete burn-off within 600 °C.[2,119]

Electrospinning is a technique to produce fine fibers by charging a polymer melt or solution under high voltages. The high voltage counteracts the surface tension of the fluid to form a thin fiber or filament that is deposited onto a spinneret. The arrangement of these fibers on the spinneret will dictate the porous volume of the surface structure. Electrospinning can produce fibers at the nanometric level, which can mimic the features present in natural bone. For example, Xu et al.[120] produced a 3D electro-spun scaffold with hierarchical porosities up to 300 µm. Huang et al.[121] showed that 3D printed scaffolds with electro-spun meshes produced dual scaffolds introducing a combination of macro and micropores within the scaffold. In vitro studies showed that the activity of the scaffold was affected by fiber alignment and mesh density.[122] OCN expression showed an improvement irrespective of the processing parameters used. The anisotropic nature of the electro-spun fibers showed a positive influence over cytoskeletal attachment. However, the major limitation of electrospinning is in the production of fibers in

Table 5. Description of additive manufacturing techniques previously used to produce BTE scaffolds.

3D printing process and material	Description	Ref.
Extrusion-based 3D printing with CaP material	• Scaffolds possessed pore sizes ranging from 60 to 100 µm • Bone growth direction was determined by scaffold geometry • Instability of implanted scaffold could lead to foreign body response/formation of fibrous tissue. • Formation of thick fibrous tissue within the pores • Resorption of CaP was absent	[130]
Selective laser melting with Tantalum	• Porosity of 70% and pore size of 334 µm were used • Surface roughness of the deposited layer was higher for the Tantalum scaffold compared to the control • Higher cell proliferation on Tantalum-based scaffold • Significant difference in osteogenic markers (ALP, OPN, OCN, and Col-1) compared to the control at the 14-day mark • Tantalum scaffolds were able to maintain bone formation significantly longer than the control	[2]
Stereolithography with Biphasic CaPs	• Surface topographies on the scaffold had a mean height of 6.5 µm • Pore sizes on the biphasic CaP-based scaffold were smaller compared to the HAp (control) • Up to 72% of bone in-growth was observed after 3 months of implantation • No resorption of material was observed • Fibrous connective tissue and blood vessels were observed at the host bone and biomaterial interface	[131]
Electron beam melting with Ti-6Al-4V	• Surface defects created during the EBM process can cause a major health hazard when implanted • Nanotubes were observed on the scaffold structure after post-processing (etching and anodizing) • Presence of a smooth surface with post-process samples produced more bone at the scaffold–host interface	[132]

submicron sizes. Further, the pore sizes produced form nanoscale pores that make it impossible for the infiltration of ECM and cell migration.[123] Electrospinning can be used to process metals and ceramics indirectly, this involves preparing polymer composites containing the metal or ceramic of interest followed by post-processing the obtained nanofibers.[124]

5.1. Limitations of Conventional Manufacturing Techniques

As discussed in Sections 3 and 4, porous scaffolds used for BTE applications have specific requirements of pore sizes, shapes, and materials depending on the intended role (structural strength or interaction with ECM). Conventional manufacturing processes, as described in Figure 7, lack the required spatial control of pores and the ability to simultaneously process multiple materials. To mitigate these shortcomings, some recent studies have explored combining different materials and conventional processes at specific stages of scaffold production. For example, hydroxyapatite scaffolds were prepared by combining them with polyesters (polyol and di-isocynate) as foaming agents. This produced a porous ceramic scaffold based on the polyurethane sponge and simultaneously obtained a cellular structure due to the carbon-dioxide bubbles generated in situ. Pore sizes produced using this technique showed four major pore sizes distributed in different amounts. These major pore sizes are as follows; 1) >1 µm (less than 0.5 cc g^{-1}); 2) 4–20 µm (0.5 cc g^{-1}); 3) 20–210 µm (3 cc g^{-1}) and 4) 150–1000 µm (less than 0.5 cc g^{-1}).[125] This HAp-based scaffold with multi-scale porosities showed excellent biocompatibility. With pore formation occurring in situ, the lack of any spatial control over the porosity makes their mechanical strength unpredictable. Further, the inability to process multiple materials could impair their ability to address all the requirements of BTE scaffolds as described in Section 3.

Freeze casting, as described in Section 5 can produce porosities mimicking biological materials but only at single-length scales and directions. Previous studies have shown that, while multi-scale porosities can be achieved by utilizing different methods, establishing an interconnection between these multi-scales porosities is still a major challenge.[89,126] Specifically, in the case of BTE scaffolds where pore interconnectivity is critical for the vascularization of implanted cells responsible for the bone healing response. The design of internal and external complex features on BTE scaffolds can be a significant challenge for conventional techniques alone or even a combination. To overcome these challenges, additive manufacturing techniques have been used or incorporated into conventional techniques.

5.2. Additive Manufacturing

AM can be defined as the process of building up objects or parts layer by layer.[127] There are several techniques (as described in **Table 5**), such as fused filament fabrication, stereolithography, and selective laser sintering, which have been previously used for scaffold manufacturing across different materials.[128] Additive manufacturing techniques offer resolutions from a few microns to millimeters depending on the technique used, further, they can process polymers, ceramics, and metals.[129] The combination of AM with computer modeling enables the free-form fabrication of parts that can address the unique physiological and mechanical requirements of bone injuries or defects.

In vivo studies involving the implantation of a CaP 3D-printed scaffold into the patient's cleft showed increased bone growth when the gap between the host bone and the scaffold was minimal (shown in **Figure 8**I). Therefore, the patient-specific 3D-printed implant contributed toward a faster healing response by accurately filling the gap between the fractured ends. Changing

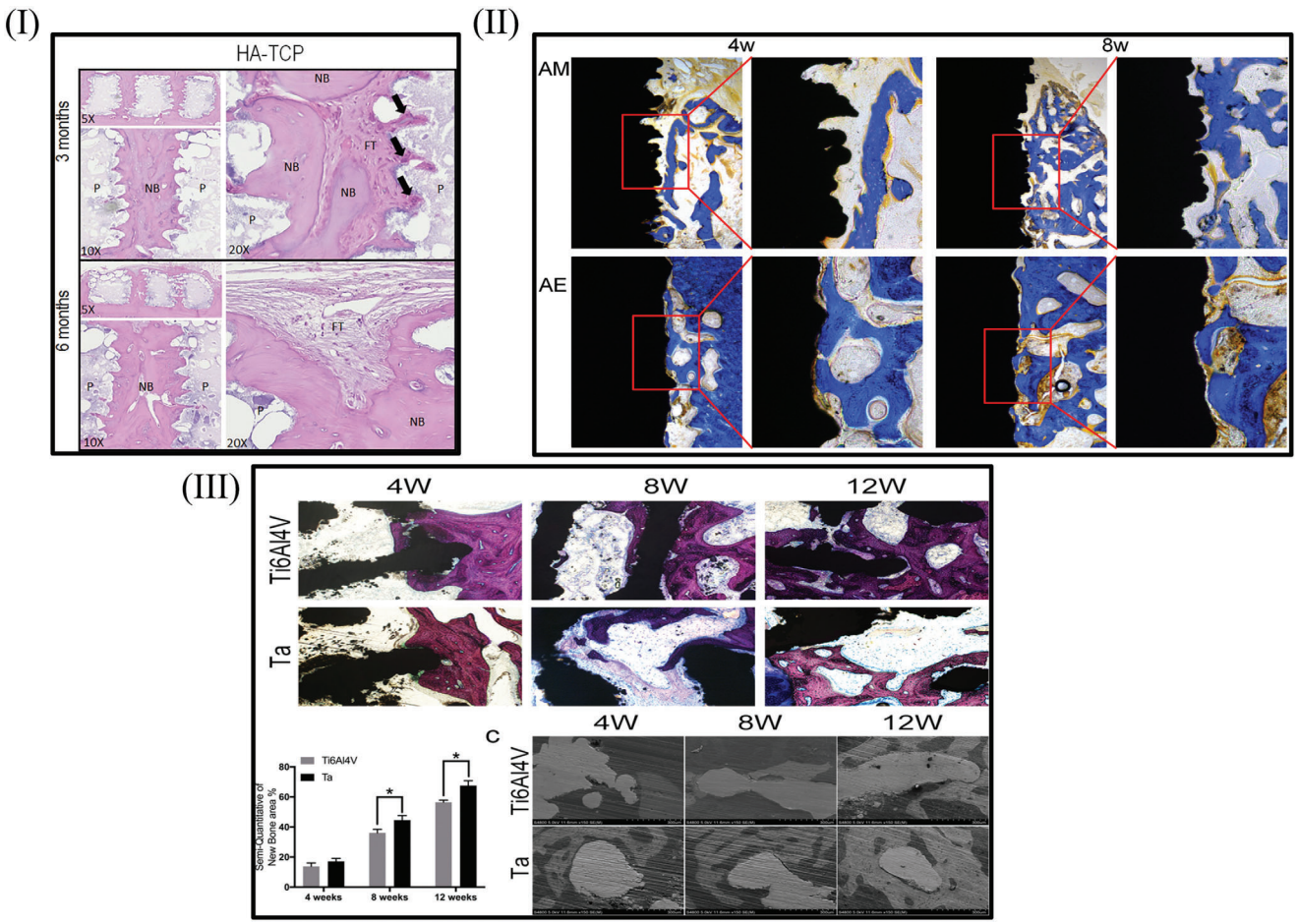

Figure 8. I) HAp-TCP-based scaffolds show positive interaction with local ECM forming new bone (NB) that is integrated with the existing bone. Presence of fibrous tissue at the interface of the new and existing bone indicates that an early foreign body response was initiated. Reproduced with permission.[131] Copyright 2020, Wiley Periodicals, LLC. II) Histological staining of a Ti-6Al-4V-based scaffold prepared using electron beam melting showed the formation of new bone tissue within 4 weeks of implantation. Anodic oxidation of the surface showed an improved bone healing performance. Reproduced with permission.[132] Copyright 2021, Elsevier. III) Histological analysis of the Ta-based scaffold indicates higher new bone formation compared to Ti-6Al-4V. In the 4th week, the appearance of bone lining cells at the implanted site indicates the superior osteoinduction capabilities of the Ta-based scaffold. Further, at the 12th week, the density of new bone formed appears to be higher on the Ta-based scaffold when compared to the Ti-6Al-4V scaffold. Reproduced with permission.[2] Copyright 2019, American Chemical Society.

pore geometry from 30° to 60° showed a significantly different bone healing response and differentiation of MSCs.[130,133] A tantalum-based scaffold 3D printed using SLM showed positive responses toward bone healing (shown in Figure 8III), where the bone in-growth was enabled through the channels created during 3D printing.[2] The irregular surface created from the laser-powder interaction is known to positively influence bone healing ability and increase surface area for interaction.[2,134] 3D-printed biphasic calcium phosphates showed a significant increase in both in-growth (up to 72%) and the presence of blood vessels at the scaffold–host bone interface.[131]

Further, the irregular nature of the scaffold surface is a result of the low resolution offered by UV-based stereolithography. Hierarchical microstructure and pores created using a combination of EBM and post-processing were the primary cause for increased bone formation. Integration of the implanted tissue occurred directly with the natural bone without the formation of any fibrous connective tissue, ensuring a strong fixation (shown in Figure 8II).[132]

6. Conclusions

Discussions around the efficacy of BTE scaffolds indicate that these scaffolds require biomaterials that can positively interact with the local ECM and simultaneously provide structural support to the damaged areas. To fulfill these dual requirements, an in-depth understanding of the chemical and physical factors responsible for the initiation and continuation of the bone healing response is necessary. Since the bone healing pathway is an active area of research, designing better BTE scaffolds that can provide an ideal bone healing environment is still a challenge.

The multi-faceted requirement of BTE scaffolds makes them a complex arrangement of porosities (shapes, sizes, and interconnectivity) and biomaterials that mimic the natural structure of

bone tissue. Changes in mechanical strength requirement across different types of bone (cancellous and trabecular) and their location in the body, alters this complex arrangement. Further damages/defects presented by individuals are often unique, therefore, a one-size-fits-all approach to the manufacturing of BTE scaffolds will be less effective in improving patient outcomes.

In-vitro assessments used to validate the efficacy of the scaffold utilizes osteoblast cells, which are infiltrated into the bulk of the 3D scaffold. Increasing the geometrical complexity to address the strength and biofunctionality of the scaffold is a popular solution although visualizing the growth of the cells within the scaffold bulks (non-destructively) to assess the efficacy of the scaffold can be difficult. Bone tissues and their surrounding ECM are highly dynamic in nature, therefore, developing scaffolds that respond to either chemical or physical stimuli can be challenging. Further, the precise mechanisms that trigger and sustain bone healing processes are still an area of active research, therefore, requirements of future BTE scaffolds might change based on the results of new research. 4D printing technologies that can produce materials that respond to external stimuli could be utilized to introduce new functionalities in BTE scaffolds.

Conventional fabrication techniques are unable to capture these unique features to produce patient-specific scaffolds. Further, conventional fabrication techniques can produce hierarchical porosities that mimic natural bone structures, but they lack the ability to simultaneously process multiple materials. This increases the number of steps during the production of multi-material scaffolds that are a requirement to produce biofunctional scaffolds. In addition, they lack control over positioning the pores and features within the scaffold architecture. Since the structural capacity is closely linked with the presence of these pores, control over their spatial location can alter their structural capacity. The type of porous structure can also affect the infiltration of ECM into the scaffold, controlling the interaction of the scaffold, and hence, its bone healing ability. Therefore, by using a combination of materials and structural features, unique scaffolds with specific bone healing and structural capacities can be designed.

Recent advances in 3DP technologies combined with imaging systems (magnetic resonance image, computer tomography, and synchrotron-based CT scanning) allow us to capture and translate the unique defects/damages into scaffold designs. Incorporating finite element analysis into this design loop could allow us to predict the structural capacity of these scaffolds before manufacturing them, thereby allowing professionals to make informed decisions before implanting the scaffolds. While 3DP systems do provide significant design freedom, they are also associated with challenges in accurately replicating geometries due to poor resolutions, and materials that can be 3D printed are required to be modified (converted into slurries, pastes, filaments, or powder). More knowledge is required to understand the impact of these modifications on bone healing ability or even their mechanical strength. When processing multiple materials using 3DP, the interaction of dissimilar materials can create defects (cracks or residual stresses) further the adhesion between the materials will be a critical factor when determining the mechanical strength of the produced composite. These knowledge gaps will need to be addressed to truly produce the next generation of patient-tailored BTE scaffolds.

Supporting Information

Supporting Information is available from the Wiley Online Library or from the author.

Acknowledgements

Open access publishing facilitated by James Cook University, as part of the Wiley - James Cook University agreement via the Council of Australian University Librarians.

Conflict of Interest

The authors declare no conflict of interest.

Keywords

biomaterials, bone tissue engineering, hierarchical structures

Received: October 26, 2022
Revised: November 29, 2022
Published online: January 22, 2023

[1] a) L. Claes, P. Augat, G. Suger, H. J. Wilke, *J. Orthop. Res.* **1997**, *15*, 577; b) S. Verrier, M. Alini, E. Alsberg, S. Buchman, D. Kelly, M. Laschke, M. Menger, W. Murphy, J. Stegemann, M. Schütz, *Eur. Cell Mater.* **2016**, *32*, 87.
[2] a) P. Balasubramanian, A. Grünewald, R. Detsch, L. Hupa, B. Jokic, F. Tallia, A. K. Solanki, J. R. Jones, A. R. Boccaccini, *Int. J. Appl. Glass Sci.* **2016**, *7*, 206; b) R. Dwivedi, S. Kumar, R. Pandey, A. Mahajan, D. Nandana, D. S. Katti, D. Mehrotra, *J. Oral Biol. Craniofacial Res.* **2020**, *10*, 381; c) Y. Guo, K. Xie, W. Jiang, L. Wang, G. Li, S. Zhao, W. Wu, Y. Hao, *ACS Biomater. Sci. Eng.* **2019**, *5*, 1123.
[3] M. Rahmati, E. A. Silva, J. E. Reseland, C. A. Heyward, H. J. Haugen, *Chem. Soc. Rev.* **2020**, *49*, 5178.
[4] S. Spiller, F. Clauder, K. Bellmann-Sickert, A. G. Beck-Sickinger, *Biol. Chem.* **2021**, *402*, 1271.
[5] T. Albrektsson, C. Johansson, *Eur. Spine J.* **2001**, *10*, S96.
[6] Y. Ha, X. Ma, S. Li, T. Li, Z. Li, Y. Qian, M. Shafiq, J. Wang, X. Zhou, C. He, *Adv. Funct. Mater.* **2022**, *32*, 2200011.
[7] a) Y. Liu, D. Luo, T. Wang, *Small* **2016**, *12*, 4611; b) R. Florencio-Silva, G. R. da Silva Sasso, E. Sasso-Cerri, M. J. Simões, P. S. Cerri, *Biomed Res. Int.* **2015**, *2015*, 421746; c) H. Follet, G. Boivin, C. Rumelhart, P. Meunier, *Bone* **2004**, *34*, 783.
[8] a) S. Samavedi, A. R. Whittington, A. S. Goldstein, *Acta Biomater.* **2013**, *9*, 8037; b) H. Ma, C. Feng, J. Chang, C. Wu, *Acta Biomater.* **2018**, *79*, 37; c) H. Jodati, B. Yılmaz, Z. Evis, *Ceram. Int.* **2020**, *46*, 15725.
[9] H. Qu, H. Fu, Z. Han, Y. Sun, *RSC Adv.* **2019**, *9*, 26252.
[10] a) S. Zhang, S. Vijayavenkataraman, W. F. Lu, J. Y. H. Fuh, *J. Biomed. Mater. Res., Part B* **2019**, *107*, 1329; b) A. Wubneh, E. K. Tsekoura, C. Ayranci, H. Uludağ, *Acta Biomater.* **2018**, *80*, 1.
[11] X. Su, T. Wang, S. Guo, *Regener. Ther.* **2021**, *16*, 63.
[12] a) A. P. M. Madrid, S. M. Vrech, M. A. Sanchez, A. P. Rodriguez, *Mater. Sci. Eng., C* **2019**, *100*, 631; b) X. Zhou, Y. Feng, J. Zhang, Y. Shi, L. Wang, *Int. J. Adv. Manuf. Technol.* **2020**, *108*, 3591.
[13] H. C. Anderson, *J. Cell Biol.* **1969**, *41*, 59.
[14] a) T. Hasegawa, T. Yamamoto, E. Tsuchiya, H. Hongo, K. Tsuboi, A. Kudo, M. Abe, T. Yoshida, T. Nagai, N. Khadiza, A. Yokoyama, K. Oda, H. Ozawa, P. H. L. de Freitas, M. Li, N. Amizuka, *Jpn. Dent. Sci. Rev.* **2017**, *53*, 34; b) H. C. Anderson, J. J. Reynolds, *Dev. Biol.* **1973**, *34*, 211.

[15] D. G. Walker, *Science* **1973**, *180*, 875.
[16] A. M. Mohamed, *Malays. J. Med. Sci.* **2008**, *15*, 4.
[17] J. Rouwkema, N. C. Rivron, C. A. van Blitterswijk, *Trends Biotechnol.* **2008**, *26*, 434.
[18] W. Risau, *Nature* **1997**, *386*, 671.
[19] U. G. K. Wegst, H. Bai, E. Saiz, A. P. Tomsia, R. O. Ritchie, *Nat. Mater.* **2015**, *14*, 23.
[20] S. K. Ramchand, E. Seeman, *Curr. Osteoporos. Rep.* **2018**, *16*, 561.
[21] J.-Y. Rho, L. Kuhn-Spearing, P. Zioupos, *Med. Eng. Phys.* **1998**, *20*, 92.
[22] C. Micheletti, A. Hurley, A. Gourrier, A. Palmquist, T. Tang, F. A. Shah, K. Grandfield, *Acta Biomater.* **2022**, *142*, 1.
[23] Boundless, in General Biology, (Ed: Boundless), Libretexts, LibreTexts Biology **2022**.
[24] D. H. Pahr, A. G. Reisinger, *Curr. Osteoporos. Rep.* **2020**, *18*, 696.
[25] M. Maruyama, C. Rhee, T. Utsunomiya, N. Zhang, M. Ueno, Z. Yao, S. B. Goodman, *Front. Endocrinol.* **2020**, *11*, 386.
[26] S. Nassiri, P. Graney, K. L. Spiller, in *A Tissue Regeneration Approach to Bone and Cartilage Repair*, Springer, New York **2015**, pp. 65–84.
[27] J. Lee, H. Byun, S. K. M. Perikamana, S. Lee, H. Shin, *Adv. Healthcare Mater.* **2019**, *8*, 1800861.
[28] A. Shekaran, A. J. García, *J. Biomed. Mater. Res., Part A* **2011**, *96*, 261.
[29] G. Zhu, T. Zhang, M. Chen, K. Yao, X. Huang, B. Zhang, Y. Li, J. Liu, Y. Wang, Z. Zhao, *Bioact. Mater.* **2021**, *6*, 4110.
[30] B. Langdahl, S. Ferrari, D. W. Dempster, *Ther. Adv. Musculoskeletal Dis.* **2016**, *8*, 225.
[31] M. Ansari, *Prog. Biomater.* **2019**, *8*, 223.
[32] P. Katsimbri, *Eur. J. Cancer Care* **2017**, *26*, e12740.
[33] J.-M. Kim, C. Lin, Z. Stavre, M. B. Greenblatt, J.-H. Shim, *Cells* **2020**, *9*, 2073.
[34] X. Lin, S. Patil, Y.-G. Gao, A. Qian, *Front. Pharmacol.* **2020**, *11*, 757.
[35] M. Kerschnitzki, W. Wagermaier, P. Roschger, J. Seto, R. Shahar, G. N. Duda, S. Mundlos, P. Fratzl, *J. Struct. Biol.* **2011**, *173*, 303.
[36] J. Gluhak-Heinrich, L. Ye, L. F. Bonewald, J. Q. Feng, M. MacDougall, S. E. Harris, D. Pavlin, *J. Bone Miner. Res.* **2003**, *18*, 807.
[37] M. Matsumoto, C. Biguetti, A. Fonseca, P. Saraiva, *J. Mol. Signaling Updates* **2016**, *1*, 33.
[38] Y. Zhou, C. Wu, J. Chang, *Mater. Today* **2019**, *24*, 41.
[39] a) J. Grech, E. Antunes, *J. Mater. Res. Technol.* **2019**, *8*, 4956; b) T. Munro, C. M. Miller, E. Antunes, D. Sharma, *J. Funct. Biomater.* **2020**, *11*, 50.
[40] a) C. Zhang, F. Wang, Z. Jiang, J. Lan, L. Zhao, P. Si, *Ceram. Int.* **2021**, *47*, 6940; b) J. Grech, E. Antunes, *Ceram. Int.* **2020**, *46*, 24792.
[41] M. Merola, S. Affatato, *Materials* **2019**, *12*, 495.
[42] E. P. Erasmus, R. Sule, O. T. Johnson, J. Massera, I. Sigalas, *Sci. Rep.* **2018**, *8*, 3699.
[43] R. G. Ribas, V. M. Schatkoski, T. L. do Amaral Montanheiro, B. R. C. de Menezes, C. Stegemann, D. M. G. Leite, G. P. Thim, *Ceram. Int.* **2019**, *45*, 21051.
[44] a) S. Gomes, C. Vichery, S. Descamps, H. Martinez, A. Kaur, A. Jacobs, J.-M. Nedelec, G. Renaudin, *Acta Biomater.* **2018**, *65*, 462; b) C. Wu, Y. Zhou, M. Xu, P. Han, L. Chen, J. Chang, Y. Xiao, *Biomaterials* **2013**, *34*, 422.
[45] a) R. Ballouze, M. H. Marahat, S. Mohamad, N. A. Saidin, S. R. Kasim, J. P. Ooi, *J. Biomed. Mater. Res., Part B* **2021**, *109*, 1426; b) T. Qi, J. Weng, F. Yu, W. Zhang, G. Li, H. Qin, Z. Tan, H. Zeng, *Biol. Trace Elem. Res.* **2021**, *199*, 559.
[46] a) T. Wu, H. Shi, Y. Liang, T. Lu, Z. Lin, J. Ye, *Mater. Sci. Eng., C* **2020**, *109*, 110481; b) K. Sule, J. Umbsaar, E. J. Prenner, *Biochim. Biophys. Acta Biomembr.* **2020**, *1862*, 183250.
[47] G. Hulsart-Billström, W. Xia, E. Pankotai, M. Weszl, E. Carlsson, C. Forster-Horváth, S. Larsson, H. Engqvist, Z. Lacza, *J. Biomed. Mater. Res., Part A* **2013**, *101A*, 2322.
[48] J. Cao, R. Lian, X. Jiang, A. V. Rogachev, *Surf. Coat. Technol.* **2021**, *416*, 127177.
[49] J. Lu, H. Yu, C. Chen, *RSC Adv.* **2018**, *8*, 2015.
[50] L. Guo, Z. Liang, L. Yang, W. Du, T. Yu, H. Tang, C. Li, H. Qiu, *J. Controlled Release* **2021**, *338*, 571.
[51] Y. Li, Y. Liu, R. Li, H. Bai, Z. Zhu, L. Zhu, C. Zhu, Z. Che, H. Liu, J. Wang, L. Huang, *Mater. Des.* **2021**, *210*, 110049.
[52] S. Sharma, P. Sudhakara, J. Singh, R. A. Ilyas, M. R. M. Asyraf, M. R. Razman, *Polymers* **2021**, *13*, 2623.
[53] F. Zhang, M. W. King, *Adv. Healthcare Mater.* **2020**, *9*, 1901358.
[54] A. C. B. Benatti, A. F. Pattaro, A. A. Rodrigues, M. V. Xavier, A. Kaasi, M. I. R. Barbosa, A. L. Jardini, R. M. Filho, P. Kharmandayan, in *Materials for Biomedical Engineering* (Eds: A.-M. Holban, A. M. Grumezescu), Elsevier, New York **2019**, pp. 83–116.
[55] F. Ghorbani, M. Sahranavard, Z. M. Nejad, D. Li, A. Zamanian, B. Yu, *Front. Mater.* **2020**, *7*, 528590.
[56] T. N. Vo, F. K. Kasper, A. G. Mikos, *Adv. Drug Delivery Rev.* **2012**, *64*, 1292.
[57] a) D. Sun, Y. Chen, R. T. Tran, S. Xu, D. Xie, C. Jia, Y. Wang, Y. Guo, Z. Zhang, J. Guo, J. Yang, D. Jin, X. Bai, *Sci. Rep.* **2014**, *4*, 6912; b) E. Davies, K. H. Müller, W. C. Wong, C. J. Pickard, D. G. Reid, J. N. Skepper, M. J. Duer, *Proc. Natl. Acad. Sci. USA* **2014**, *111*, E1354.
[58] a) B. N. Teixeira, P. Aprile, R. H. Mendonça, D. J. Kelly, R. M. d. S. M. Thiré, *J. Biomed. Mater. Res., Part B* **2019**, *107*, 37; b) H.-j. Cho, S. K. M. Perikamana, J.-h. Lee, J. Lee, K.-M. Lee, C. S. Shin, H. Shin, *ACS Appl. Mater. Interfaces* **2014**, *6*, 11225.
[59] A. M. Cakmak, S. Unal, A. Sahin, F. N. Oktar, M. Sengor, N. Ekren, O. Gunduz, D. M. Kalaskar, *Polymers* **2020**, *12*, 1962.
[60] B. Vaidhyanathan, P. Vincent, S. Vadivel, P. Karuppiah, N. A. Al-Dhabi, D. R. Sadhasivam, S. Vimalraj, S. Saravanan, *Process Biochem.* **2021**, *100*, 178.
[61] M. Rasoulianboroujeni, F. Fahimipour, P. Shah, K. Khoshroo, M. Tahriri, H. Eslami, A. Yadegari, E. Dashtimoghadam, L. Tayebi, *Mater. Sci. Eng., C* **2019**, *96*, 105.
[62] I. K. Januariyasa, I. D. Ana, Y. Yusuf, *Mater. Sci. Eng., C* **2020**, *107*, 110347.
[63] C. Shuai, Z. Zeng, Y. Yang, F. Qi, S. Peng, W. Yang, C. He, G. Wang, G. Qian, *Mater. Des.* **2020**, *190*, 108564.
[64] R. Eivazzadeh-Keihan, E. B. Noruzi, K. K. Chenab, A. Jafari, F. Radinekiyan, S. M. Hashemi, F. Ahmadpour, A. Behboudi, J. Mosafer, A. Mokhtarzadeh, A. Maleki, M. R. Hamblin, *J. Tissue Eng. Regener. Med.* **2020**, *14*, 1687.
[65] M. Geetha, A. K. Singh, R. Asokamani, A. K. Gogia, *Prog. Mater. Sci.* **2009**, *54*, 397.
[66] a) S. Wang, L. Liu, K. Li, L. Zhu, J. Chen, Y. Hao, *Mater. Des.* **2019**, *168*, 107643; b) W. Xu, J. Tian, Z. Liu, X. Lu, M. D. Hayat, Y. Yan, Z. Li, X. Qu, C. Wen, *Mater. Sci. Eng., C* **2019**, *105*, 110015.
[67] W. Xu, X. Lu, M. D. Hayat, J. Tian, C. Huang, M. Chen, X. Qu, C. Wen, *J. Mater. Res. Technol.* **2019**, *8*, 3696.
[68] a) M. Cassandri, A. Smirnov, F. Novelli, C. Pitolli, M. Agostini, M. Malewicz, G. Melino, G. Raschellà, *Cell Death Discovery* **2017**, *3*, 17071; b) Y. Su, I. Cockerill, Y. Wang, Y.-X. Qin, L. Chang, Y. Zheng, D. Zhu, *Trends Biotechnol.* **2019**, *37*, 428.
[69] I. Cockerill, Y. Su, S. Sinha, Y.-X. Qin, Y. Zheng, M. L. Young, D. Zhu, *Mater. Sci. Eng., C* **2020**, *110*, 110738.
[70] S. Kamrani, C. Fleck, *BioMetals* **2019**, *32*, 185.
[71] E. Dayaghi, H. R. Bakhsheshi-Rad, E. Hamzah, A. Akhavan-Farid, A. F. Ismail, M. Aziz, E. Abdolahi, *Mater. Sci. Eng., C* **2019**, *102*, 53.
[72] D. N. Heo, W.-K. Ko, M. S. Bae, J. B. Lee, D.-W. Lee, W. Byun, C. H. Lee, E.-C. Kim, B.-Y. Jung, I. K. Kwon, *J. Mater. Chem. B* **2014**, *2*, 1584.
[73] J. Zhang, D. Huang, S. Liu, X. Dong, Y. Li, H. Zhang, Z. Yang, Q. Su, W. Huang, W. Zheng, W. Zhou, *Mater. Sci. Eng., C* **2019**, *105*, 110054.
[74] D. Arcos, M. Vallet-Regí, *J. Mater. Chem. B* **2020**, *8*, 1781.

[75] M. Rizwan, M. Hamdi, W. J. Basirun, *J. Biomed. Mater. Res., Part A* **2017**, *105*, 3197.
[76] a) L. Gritsch, M. Maqbool, V. Mouriño, F. E. Ciraldo, M. Cresswell, P. R. Jackson, C. Lovell, A. R. Boccaccini, *J. Mater. Chem. B* **2019**, *7*, 6109; b) P. J. Marie, P. Ammann, G. Boivin, C. Rey, *Calcif. Tissue Int.* **2001**, *69*, 121.
[77] G. Grass, C. Rensing, M. Solioz, *Appl. Environ. Microbiol.* **2011**, *77*, 1541.
[78] a) C. X. F. Lam, X. M. Mo, S. H. Teoh, D. W. Hutmacher, *Mater. Sci. Eng., C* **2002**, *20*, 49; b) C. Koski, B. Onuike, A. Bandyopadhyay, S. Bose, *Addit. Manuf.* **2018**, *24*, 47.
[79] a) M. N. Collins, G. Ren, K. Young, S. Pina, R. L. Reis, J. M. Oliveira, *Adv. Funct. Mater.* **2021**, *31*, 2010609; b) N. Betancourt, X. Chen, *Bioprinting* **2022**, *25*, e00189; c) H. Ravanbakhsh, V. Karamzadeh, G. Bao, L. Mongeau, D. Juncker, Y. S. Zhang, *Adv. Mater.* **2021**, *33*, 2104730.
[80] S. Dutta, K. B. Devi, S. Mandal, A. Mahato, S. Gupta, B. Kundu, V. K. Balla, M. Roy, *Materialia* **2019**, *5*, 100245.
[81] a) Y. Wan, T. Cui, W. Li, C. Li, J. Xiao, Y. Zhu, D. Ji, G. Xiong, H. Luo, *Mater. Des.* **2016**, *99*, 521; b) M. Khodaei, F. Nejatidanesh, M. J. Shirani, A. Valanezhad, I. Watanabe, O. Savabi, *J. Mech. Behav. Biomed. Mater.* **2019**, *100*, 103396.
[82] G. Iviglia, S. Kargozar, F. Baino, *J. Funct. Biomater.* **2019**, *10*, 3.
[83] Y. Sugawara, H. Kamioka, T. Honjo, K.-i. Tezuka, T. Takano-Yamamoto, *Bone* **2005**, *36*, 877.
[84] Z. B. Velioglu, D. Pulat, B. Demirbakan, B. Ozcan, E. Bayrak, C. Erisken, *Connect. Tissue Res.* **2019**, *60*, 274.
[85] M. J. Gupte, W. B. Swanson, J. Hu, X. Jin, H. Ma, Z. Zhang, Z. Liu, K. Feng, G. Feng, G. Xiao, N. Hatch, Y. Mishina, P. X. Ma, *Acta Biomater.* **2018**, *82*, 1.
[86] a) H. J. Haugen, S. P. Lyngstadaas, F. Rossi, G. Perale, *J. Clin. Periodontol.* **2019**, *46*, 92; b) C. Ghayor, F. E. Weber, *Front. Physiol.* **2018**, *9*, 960.
[87] H. Zhao, L. Li, S. Ding, C. Liu, J. Ai, *Mater. Lett.* **2018**, *223*, 21.
[88] a) L. Morejón, J. A. Delgado, A. A. Ribeiro, M. V. de Oliveira, E. Mendizábal, I. García, A. Alfonso, P. Poh, M. van Griensven, E. R. Balmayor, *Int. J. Mol. Sci.* **2019**, *20*, 1790; b) P. Diaz-Rodriguez, M. Sánchez, M. Landin, *Pharmaceutics* **2018**, *10*, 272.
[89] J.-Y. Jung, S. E. Naleway, Y. N. Maker, K. Y. Kang, J. Lee, J. Ha, S. S. Hur, S. Chien, J. McKittrick, *ACS Biomater. Sci. Eng.* **2019**, *5*, 2122.
[90] S. Bose, M. Roy, A. Bandyopadhyay, *Trends Biotechnol.* **2012**, *30*, 546.
[91] C. M. Murphy, M. G. Haugh, F. J. O'Brien, *Biomaterials* **2010**, *31*, 461.
[92] N. Abbasi, S. Hamlet, R. M. Love, N.-T. Nguyen, *J. Sci.: Adv. Mater. Devices* **2020**, *5*, 1.
[93] S. Kanwar, O. Al-Ketan, S. Vijayavenkataraman, *Mater. Des.* **2022**, *220*, 110857.
[94] D. Bicho, R. F. Canadas, C. Gonçalves, S. Pina, R. L. Reis, J. M. Oliveira, *J. Biomater. Sci. Polym. Ed.* **2021**, *32*, 1966.
[95] a) C. Gao, S. Peng, P. Feng, C. Shuai, *Bone Res.* **2017**, *5*, 17059; b) A. Arora, A. Kothari, D. S. Katti, *J. Mech. Behav. Biomed. Mater.* **2015**, *51*, 169.
[96] a) J. A. Sanz-Herrera, J. M. García-Aznar, M. Doblaré, *Acta Biomater.* **2009**, *5*, 219; b) F. J. O'Brien, B. A. Harley, M. A. Waller, I. V. Yannas, L. J. Gibson, P. J. Prendergast, *Technol. Health Care* **2007**, *15*, 3; c) M. R. Dias, P. R. Fernandes, J. M. Guedes, S. J. Hollister, *J. Biomech.* **2012**, *45*, 938.
[97] a) A. P. G. Castro, J. Santos, T. Pires, P. R. Fernandes, *Macromol. Mater. Eng.* **2020**, *305*, 2000487; b) A. P. G. Castro, T. Pires, J. E. Santos, B. P. Gouveia, P. R. Fernandes, *Materials* **2019**, *12*, 1313.
[98] A. Yánez, A. Cuadrado, O. Martel, H. Afonso, D. Monopoli, *Mater. Des.* **2018**, *140*, 21.
[99] a) A. Ataee, Y. Li, M. Brandt, C. Wen, *Acta Mater.* **2018**, *158*, 354; b) M. Alizadeh-Osgouei, Y. Li, A. Vahid, A. Ataee, C. Wen, *Smart Mater. Med.* **2021**, *2*, 15; c) C. N. Kelly, J. Francovich, S. Julmi, D. Safranski, R. E. Guldberg, H. J. Maier, K. Gall, *Acta Biomater.* **2019**, *94*, 610.
[100] Y. Zheng, Q. Han, D. Li, F. Sheng, Z. Song, J. Wang, *Mater. Des.* **2021**, *197*, 109219.
[101] Q. Zhang, L. Ma, X. Ji, Y. He, Y. Cui, X. Liu, C. Xuan, Z. Wang, W. Yang, M. Chai, X. Shi, *Adv. Funct. Mater.* **2022**, *32*, 2204182.
[102] S. Rajagopalan, R. A. Robb, *Med. Image Anal.* **2006**, *10*, 693.
[103] L. Zhang, S. Feih, S. Daynes, S. Chang, M. Y. Wang, J. Wei, W. F. Lu, *Addit. Manuf.* **2018**, *23*, 505.
[104] S. Yu, J. Sun, J. Bai, *Mater. Des.* **2019**, *182*, 108021.
[105] L. Yuan, S. Ding, C. Wen, *Bioact. Mater.* **2019**, *4*, 56.
[106] N. Novak, O. Al-Ketan, M. Borovinšek, L. Krstulović-Opara, R. Rowshan, M. Vesenjak, Z. Ren, *J. Mater. Res. Technol.* **2021**, *15*, 1318.
[107] O. Al-Ketan, R. Rowshan, R. K. Abu Al-Rub, *Addit. Manuf.* **2018**, *19*, 167.
[108] L. Han, S. Che, *Adv. Mater.* **2018**, *30*, 1705708.
[109] M. Xu, H. Li, D. Zhai, J. Chang, S. Chen, C. Wu, *J. Mater. Chem. B* **2015**, *3*, 3799.
[110] C. Lei, Y. Cao, S. Hosseinpour, F. Gao, J. Liu, J. Fu, R. Staples, S. Ivanovski, C. Xu, *Nano Res.* **2021**, *14*, 770.
[111] J. Lee, G. Kim, *ACS Appl. Mater. Interfaces* **2018**, *10*, 35801.
[112] T. Ohji, M. Fukushima, *Int. Mater. Rev.* **2012**, *57*, 115.
[113] a) B. R. Thompson, T. S. Horozov, S. D. Stoyanov, V. N. Paunov, *J. Mater. Chem. A* **2019**, *7*, 8030; b) H. Tetik, Y. Wang, X. Sun, D. Cao, N. Shah, H. Zhu, F. Qian, D. Lin, *Adv. Funct. Mater.* **2021**, *31*, 2103410; c) Y. Chen, W. Li, C. Zhang, Z. Wu, J. Liu, *Adv. Healthcare Mater.* **2020**, *9*, 2000724.
[114] F. Ghorbani, H. Nojehdehian, A. Zamanian, *Mater. Sci. Eng., C* **2016**, *69*, 208.
[115] H. Lee, T.-S. Jang, J. Song, H.-E. Kim, H.-D. Jung, *Materials* **2017**, *10*, 367.
[116] I. Himoto, S. Yamashita, H. Kita, *Adv. Powder Technol.* **2016**, *27*, 948.
[117] a) D. Desimone, W. Li, J. A. Roether, D. W. Schubert, M. C. Crovace, A. C. M. Rodrigues, E. D. Zanotto, A. R. Boccaccini, *Sci. Technol. Adv. Mater.* **2013**, *14*, 045008; b) K. Bodišová, M. Kašiarová, M. Domanická, M. Hnatko, Z. Lenčéš, Z. V. Nováková, J. Vojtaššák, S. Gromošová, P. Šajgalík, *Ceram. Int.* **2013**, *39*, 8355; c) J.-H. Sung, K.-H. Shin, Y.-W. Moon, Y.-H. Koh, W.-Y. Choi, H.-E. Kim, *Ceram. Int.* **2012**, *38*, 93.
[118] a) V. Karageorgiou, D. Kaplan, *Biomaterials* **2005**, *26*, 5474; b) M. Kim, R. A. Franco, B.-T. Lee, *J. Eur. Ceram. Soc.* **2011**, *31*, 1541.
[119] a) O. M. Goudouri, E. Theodosoglou, E. Kontonasaki, J. Will, K. Chrissafis, P. Koidis, K. M. Paraskevopoulos, A. R. Boccaccini, *Mater. Res. Bull.* **2014**, *49*, 399; b) Z. Sun, Y. Liang, M. Li, Y. Zhou, *J. Am. Ceram. Soc.* **2010**, *93*, 2591; c) D. Loca, I. Narkevica, J. Ozolins, *Mater. Lett.* **2015**, *159*, 309.
[120] T. Xu, J. M. Miszuk, Y. Zhao, H. Sun, H. Fong, *Adv. Healthcare Mater.* **2015**, *4*, 2238.
[121] B. Huang, E. Aslan, Z. Jiang, E. Daskalakis, M. Jiao, A. Aldalbahi, C. Vyas, P. Bártolo, *Addit. Manuf.* **2020**, *36*, 101452.
[122] S. Sankar, C. S. Sharma, S. N. Rath, S. Ramakrishna, *J. Tissue Eng. Regener. Med.* **2018**, *12*, e604.
[123] Y. Yu, S. Hua, M. Yang, Z. Fu, S. Teng, K. Niu, Q. Zhao, C. Yi, *RSC Adv.* **2016**, *6*, 110557.
[124] W. Sigmund, J. Yuh, H. Park, V. Maneeratana, G. Pyrgiotakis, A. Daga, J. Taylor, J. C. Nino, *J. Am. Ceram. Soc.* **2006**, *89*, 395.
[125] L. Novotna, L. Kucera, A. Hampl, D. Drdlik, J. Cihlar, J. Cihlar, *Mater. Sci. Eng., C* **2019**, *95*, 363.
[126] a) H. Bai, D. Wang, B. Delattre, W. Gao, J. De Coninck, S. Li, A. P. Tomsia, *Acta Biomater.* **2015**, *20*, 113; b) H.-D. Jung, S.-W. Yook, H.-E. Kim, Y.-H. Koh, *Mater. Lett.* **2009**, *63*, 1545; c) W. Li, M. M. Porter, E. A. Olevsky, R. M. German, J. McKittrick, *Mater. Sci. Eng., A* **2015**, *636*, 148.
[127] M. McFarland, E. Antunes, *Aerospace* **2019**, *6*, 81.

[128] a) Z. Wang, Y. Wang, J. Yan, K. Zhang, F. Lin, L. Xiang, L. Deng, Z. Guan, W. Cui, H. Zhang, *Adv. Drug Delivery Rev.* **2021**, *174*, 504; b) L. Zhang, G. Yang, B. N. Johnson, X. Jia, *Acta Biomater.* **2019**, *84*, 16; c) X. Hu, Z. Lin, J. He, M. Zhou, S. Yang, Y. Wang, K. Li, *MedComm* **2022**, *1*, e14; d) A. Koyyada, P. Orsu, *Regener. Eng. Transl. Med.* **2021**, *7*, 147.
[129] G. Liu, X. Zhang, X. Chen, Y. He, L. Cheng, M. Huo, J. Yin, F. Hao, S. Chen, P. Wang, S. Yi, L. Wan, Z. Mao, Z. Chen, X. Wang, Z. Cao, J. Lu, *Mater. Sci. Eng., R* **2021**, *145*, 100596.
[130] P. Korn, T. Ahlfeld, F. Lahmeyer, D. Kilian, P. Sembdner, R. Stelzer, W. Pradel, A. Franke, M. Rauner, U. Range, *Front. Bioeng. Biotechnol.* **2020**, *8*, 217.
[131] L. Le Guéhennec, D. Van hede, E. Plougonven, G. Nolens, B. Verlée, M.-C. De Pauw, F. Lambert, *J. Biomed. Mater. Res., Part A* **2020**, *108*, 412.
[132] B. Ren, Y. Wan, C. Liu, H. Wang, M. Yu, X. Zhang, Y. Huang, *Mater. Sci. Eng., C* **2021**, *118*, 111505.
[133] A. Di Luca, I. Lorenzo-Moldero, C. Mota, A. Lepedda, D. Auhl, C. Van Blitterswijk, L. Moroni, *Adv. Healthcare Mater.* **2016**, *5*, 1753.
[134] Z. Schwartz, K. Kieswetter, D. D. Dean, B. D. Boyan, *J. Periodontal. Res.* **1997**, *32*, 166.
[135] Y. Chen, N. Kawazoe, G. Chen, *Acta Biomater.* **2018**, *67*, 341.
[136] X. Wang, Y. Liu, M. Zhang, D. Zhai, Y. Wang, H. Zhuang, B. Ma, Y. Qu, X. Yu, J. Ma, H. Ma, Q. Yao, C. Wu, *Adv. Healthcare Mater.* **2021**, *10*, 2101181.
[137] M. L. Gatto, M. Furlani, A. Giuliani, N. Bloise, L. Fassina, L. Visai, P. Mengucci, *Mater. Sci. Eng., C* **2021**, *128*, 112300.
[138] S.-J. Jiang, M.-H. Wang, Z.-Y. Wang, H.-L. Gao, S.-M. Chen, Y.-H. Cong, L. Yang, S.-M. Wen, D.-D. Cheng, J.-C. He, S.-H. Yu, *Adv. Funct. Mater.* **2022**, *32*, 2110931.

Tejas Mahesh Koushik is a Ph.D. student at James Cook University. His research interests lie in additive manufacturing, bone tissue engineering, patient-tailored scaffolds, lattice structures, and bioceramic composites. His Ph.D. focuses on developing novel combinations of bioceramic composites for developing patient-tailored bone tissue engineering scaffolds using stereolithography.

Catherine (Kate) Miller received her Ph.D. in parasitology from the Australian National University and is currently a senior lecturer in the College of Medicine and Dentistry at James Cook University, lecturing to dentistry students about microbiology and immunology. Her research focuses on the inflammatory response to infection and she has recently expanded her interest to include interactions between the body and materials used in bone implants.

Elsa Antunes received her Ph.D. in engineering from James Cook University and is currently a senior lecturer in the College of Science and Engineering at James Cook University, lecturing to mechanical engineering students. Her research focuses on the development of new and sustainable materials and advanced manufacturing techniques to create innovative products for different applications such as biomedical, catalysis, and environmental.